Regulatory mechanisms of HMGB1 and its receptors in polycystic ovary syndrome-driven gravid uterine inflammation

Min Hu[1,2,3], Yuehui Zhang[3,4], Yaxing Lu[1,2], Jing Han[4], Tingting Guo[4], Peng Cui[3,5], Mats Brännström[6], Linus R. Shao[3] (iD) and Håkan Billig[3]

1 Department of Traditional Chinese Medicine, The First Affiliated Hospital of Guangzhou Medical University, China
2 Institute of Integrated Traditional Chinese Medicine and Western Medicine, Guangzhou Medical University, China
3 Department of Physiology/Endocrinology, Institute of Neuroscience and Physiology, The Sahlgrenska Academy, University of Gothenburg, Sweden
4 Department of Obstetrics and Gynecology, Key Laboratory and Unit of Infertility in Chinese Medicine, First Affiliated Hospital, Heilongjiang University of Chinese Medicine, Harbin, China
5 Department of Obstetrics and Gynecology, Shuguang Hospital Affiliated to Shanghai University of Traditional Chinese Medicine, China
6 Department of Obstetrics and Gynecology, Sahlgrenska University Hospital, Sahlgrenska Academy, University of Gothenburg, Sweden

High-mobility group box 1 (HMGB1) is critical for inflammatory homeostasis and successful pregnancy, and there is a strong association among elevated levels of HMGB1, polycystic ovary syndrome (PCOS), chronic inflammation and pregnancy loss. However, the mechanisms responsible for PCOS-driven regulation of uterine HMGB1 and its candidate receptors [toll-like receptor (TLR) 2 and 4] and inflammatory responses during pregnancy remain unclear. In this study, we found a gestational stage-dependent decrease in uterine HMGB1 and TLR4 protein abundance in rats during normal pregnancy. We demonstrated that increased expression of HMGB1, TLR2 and TLR4 proteins was associated with activation of inflammation-related signalling pathways in the gravid uterus exposed to 5α-dihydrotestosterone and insulin, mimicking the clinical features (hyperandrogenism and insulin resistance) of PCOS and this elevation was completely inhibited by treatment with the androgen receptor (AR) antagonist flutamide. Interestingly, acute exposure to lipopolysaccharide suppressed HMGB1, TLR4 and inflammation-related protein abundance but did not affect androgen levels or AR expression in the gravid uterus with viable fetuses. Furthermore, immunohistochemical analysis revealed that, in addition to being localized predominately in the nuclear compartment, HMGB1 immunoreactivity was also detected in the cytoplasm in the PCOS-like rat uterus, PCOS endometrium and pregnant rat uterus with haemorrhagic and resorbed fetuses, possibly via activation of nuclear factor κB signalling. These results suggest that both AR-dependent and AR-independent mechanisms contribute to the modulation of HMGB1/TLR2/TLR4-mediated uterine inflammation. We propose that the elevation of HMGB1 and its receptors and disruption of the pro-/anti-inflammatory balance in the

gravid uterus may participate in the pathophysiology of PCOS-associated pregnancy loss.

Introduction

The worldwide prevalence of polycystic ovary syndrome (PCOS) is estimated to be 5–25% of all adolescent and reproductive-aged women across multiple geographic ancestries, ethnicities and different diagnostic criteria [1,2]. Despite the phenotypic heterogeneity of PCOS, it is undisputedly a hormone-imbalance disease and is characterized by hyperandrogenism and insulin resistance, representing a substantial health burden [3,4]. Of note, the majority of women with PCOS face a variety of fertility challenges to achieving a successful pregnancy, and women with PCOS have a greater risk for developing several pregnancy-related complications, including implantation failure or defects and miscarriage, which lead to subfertility or infertility [3,5,6]. Currently, adverse maternal decidual manifestations attributable to hyperandrogenism and insulin resistance have been put forward to explain the pathogenesis of pregnancy-related disorders in women with PCOS [6,7].

The homeostatic balance between pro- and anti-inflammatory processes in the endometrial decidua is essential for embryo implantation and successful pregnancy [8,9], whereas sustained chronic inflammation in the reproductive tissues is associated with adverse pregnancy outcomes, including implantation failure and pregnancy loss [10,11], by promoting programmed cell death such as ferroptosis [12]. Several clinical studies have shown that the onset and development of chronic, low-grade inflammation are positively linked to PCOS [13]. We and others have reported in both *in vivo* and *in vitro* experimental settings that activation of the androgen–androgen receptor (AR) axis and development of insulin resistance increase pro-inflammatory responses and are associated with elevated inflammation in different cells, such as blood mononuclear, ovarian and endometrial cells in PCOS patients and PCOS-like rats [14–18]. In addition, animal studies have demonstrated that the overactivation of uterine AR in association with increased fetal loss may be in part due to elevated gravid uterine ferroptosis under the conditions of hyperandrogenism and insulin resistance [19–21]. Despite these important findings, how the PCOS-related manifestations impact specific intracellular molecules to regulate inflammatory responses in the uterus is still not fully understood.

High-mobility group box 1 (HMGB1) is an endogenous danger signal-triggering inflammatory response protein [22,23], and it contributes to the dynamic regulation of inflammatory responses [24] and tissue repair [25] depending on its extra-nuclear [26] and extracellular localization [27]. Upon binding to receptors, including toll-like receptor (TLR) 2 and TLR4, HMGB1 activates the nuclear factor-kB (NFκB, a central regulator of inflammatory responses) signalling pathway, potentially providing a molecular mechanism for how HMGB1 contributes to the enhancement of cellular inflammatory responses by increasing multiple pro-inflammatory cytokines [23,24]. In addition to its extra-nuclear function, the nuclear localization of HMGB1 contributes to regulating gene transcription by binding to DNA in a sequence-independent manner [23]. HMGB1 is ubiquitously expressed in most mammalian tissues and cells, predominantly in the nucleus [23], and it has been reported that in human and rat endometria, strong HMGB1 immunoreactivity is localized in the nuclear compartment of epithelial and stromal cells [28,29]. With regard to its physiological function in the uterus, HMGB1 plays a critical [30] but non-exclusive role in stromal cell decidualization, embryo implantation and fertility because conditional uterine-specific knockout of *Hmgb1* in pregnant mice does not entirely abolish stromal cell decidualization, implantation or fertility [31]. In contrast, exogenous treatment with recombinant HMGB1 at gestational day (GD) 3 induces embryo implantation failure in pregnant rats [28]. Furthermore, increased levels of circulating maternal decidual and placental HMBG1 mRNA and protein are observed in women with recurrent pregnancy loss and unexplained recurrent spontaneous abortion and a mouse model of unexplained recurrent spontaneous abortion [24,32]. These findings from animal experiments and clinical studies suggest a crucial regulatory balance between the physiological roles and the detrimental effects of maternal HMGB1 on embryo implantation and pregnancy outcomes.

A growing number of clinical studies have shown that the levels of HMGB1 mRNA and protein in ovarian granulosa cells [33–36], follicular fluid [35] and serum [36–39] are higher in PCOS patients than in non-PCOS controls. This significant elevation is positively correlated with the conditions of hyperandrogenism and

insulin resistance [36,37,39]. Our laboratory and others have reported that pregnant rodents under conditions of hyperandrogenism [resulting from chronic exposure to 5α-dihydrotestosterone (DHT) or testosterone] and/ or insulin resistance (resulting from chronic exposure to insulin) exhibit aberrant expression of genes responsible for endometrial receptivity, decidualization, placentation and pro-inflammatory cytokines, and subsequently have decreased numbers of viable fetuses [40–42]. Moreover, positive correlations between TLR2 gene polymorphisms and PCOS predisposition [43] and between the elevated level of TLR4 and activation of the NFκB signalling pathway in the endometrium are seen in PCOS patients [15]. Given that pathological levels (either higher or lower than physiological levels) of maternal HMGB1 and TLRs are involved in the priming or progression of defective implantation processes and pregnancy loss [30,31,44], we hypothesized that maternal hyperandrogenism and insulin resistance trigger uterine inflammation and cause fetal loss through the induction of abnormal HMGB1, TLR2 and TLR4 protein levels in the gravid uterus during pregnancy.

In this study, we used molecular and pharmacological approaches combined with PCOS-like rat models to address the following questions: (a) Is the expression of HMGB1, TLR2 and TLR4 proteins spatiotemporally regulated in the gravid uterus under physiological conditions and in PCOS; (b) Is AR necessary for the regulation of uterine HMGB1, TLR2 and TLR4 protein expression in association with aberrant uterine inflammation and (c) Does abnormal intracellular localization of HMGB1 contribute to uterine inflammation-induced fetal loss during pregnancy? Our comprehensive analysis in this study strongly supports the relevant role of HMGB1/TLR2/ TLR4 signalling in the regulation of intrauterine inflammation during normal pregnancy and PCOS conditions.

Results

Aberrant HMGB1 immunoreactivity is associated with increased uterine inflammation in non-pregnant PCOS-like rats and PCOS patients

To assess the potential role of HMGB1 in PCOS-related uterine inflammation, we first examined intracellular HMGB1 immunoreactivity in the rat uterus and human endometrium under physiological and PCOS conditions. Consistent with previous findings [28,29], immunohistochemical studies revealed that in non-pregnant adult rats and human endometria, strong HMGB1 nuclear immunoreactivity was detected in the epithelial and stromal cells (Figs 1, 2A (upper panel), 3 (left panel) and 4A), but no or only minimal change in uterine HMGB1 immunoreactivity was detected in adult rats during the oestrus cycle (Fig. 1). Neither exogenous androgens by long-term exposure to DHT nor endogenous androgens by systemic exposure of hCG had any impact on HMGB1 nuclear immunoreactivity in the non-pregnant rat uterus (Figs 3 (right panel) and 4B). In contrast, we found that compared to controls (Fig. 4A) cytoplasmic HMGB1 immunoreactivity was increased in luminal epithelial cells, whereas nuclear HMGB1 immunoreactivity was decreased in glandular epithelial and stromal cells in the non-pregnant rat uteri exposed to insulin alone (Fig. 4C) and in those exposed to the combination of insulin and hCG (referred as PCOS-like rats [18,45]; Fig. 4D). Interestingly, we observed that compared to the non-PCOS endometrium, cytoplasmic HMGB1 immunoreactivity was also increased in endometrial glandular epithelial cells in PCOS patients with hyperandrogenism and insulin resistance (Fig. 2A (middle panel)) [46]. Furthermore, western blot analysis (Fig. 2B) showed that endometrial HMGB1 protein abundance was increased in PCOS patients with hyperandrogenism and insulin resistance compared to non-PCOS patients. Because non-pregnant PCOS-like rats and PCOS patients show activation of the NFκB signalling pathway and induction of inflammation-related gene and protein expression in the uterus [15,18,47], these findings indicate that changes in intercellular HMGB1 immunoreactivity are tightly linked to PCOS-induced uterine inflammation.

Concurrent exposure to DHT and insulin causes endocrine and metabolic abnormalities and alters uterine morphologies at GD 14.5

To assess whether long-term exposure to DHT and insulin alters endocrine and metabolic status during early and mid-pregnancy, we evaluated circulating levels of steroid hormones and glucose homeostasis in pregnant rats exposed to DHT and/or insulin at GD 14.5. As shown in Fig. 5A, DHT + INS-exposed pregnant rats exhibit increased total T levels compared to controls. Furthermore, we found that DHT + INS-exposed pregnant rats were significantly less glucose tolerant compared to controls (Fig. 5A). In addition, we observed that the levels of TNF-α, one of the insulin resistance-related inflammatory cytokines, were also increased in DHT + INS-exposed pregnant rats compared to controls (Fig. 5A). Using the same treatment setting, DHT + INS-exposed pregnant rats exhibited decreased ovarian weight and corpora lutea number
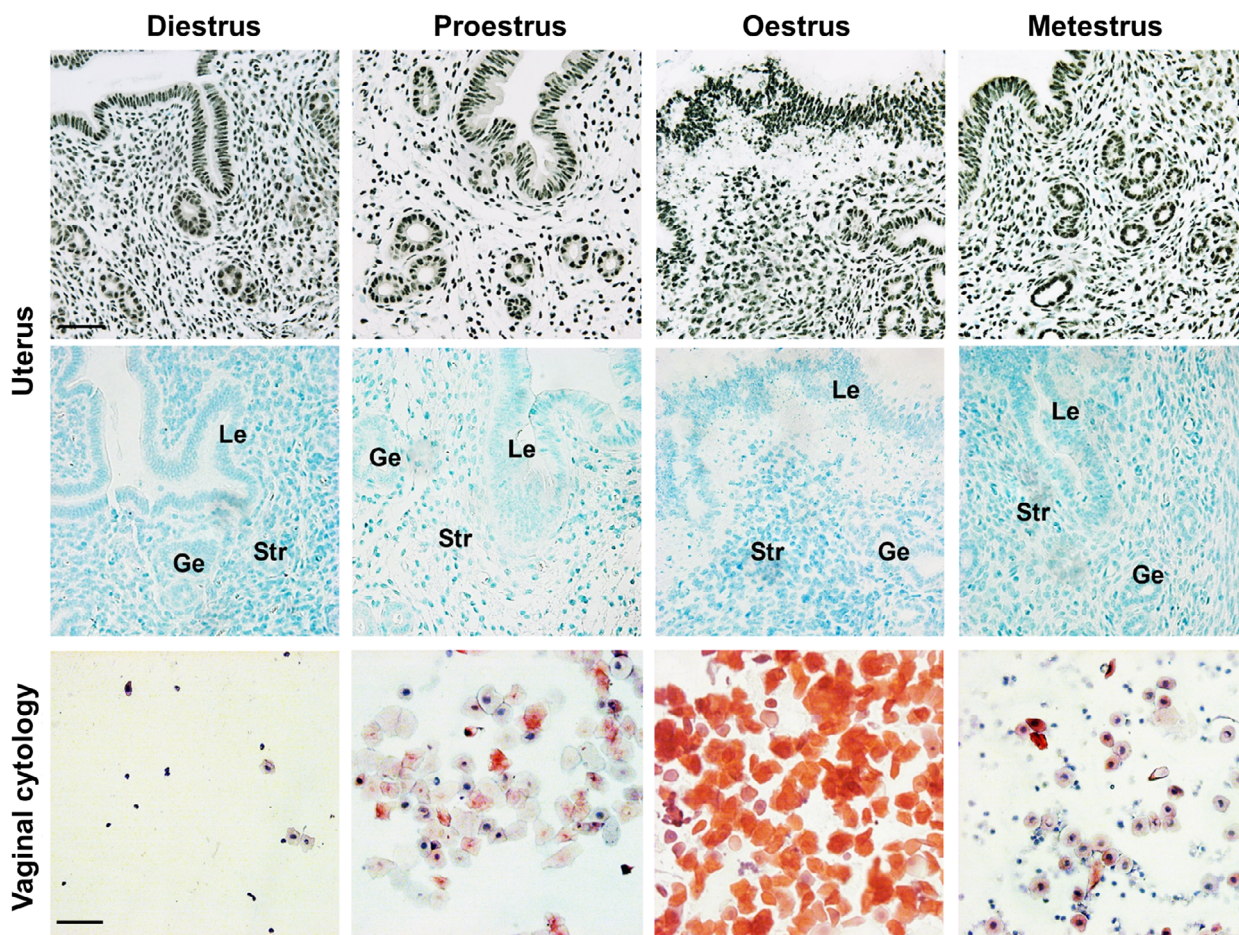
| Diestrus | Proestrus | Oestrus | Metestrus |

Fig. 1. Localization of HMGB1 protein in uteri collected from control non-pregnant rats during the oestrus cycle. Representative immunohistochemical images of intracellular HMGB1 localization. Tissue sections were counterstained with methyl green (n = 12 per group, each from different animals). Negative control staining is shown in the middle panel. Tissue sections were counterstained with methyl green. Rats were divided into four groups (dioestrus, proestrus, oestrus and metestrus) based on uterine morphology and vaginal cytology (lower panel). Ge, glandular epithelial cells; Le, luminal epithelial cells; str, stromal cells. Scale bars are 100 μm.

along with increased cyst-like ovarian follicles [48]. Thus, the significant overlaps with endocrine, metabolic and ovarian parameters between pregnant DHT + INS-treated rats and pregnant PCOS patients [49,50] indicate that concurrent exposure to DHT and insulin partially, if not entirely, reflects PCOS features both metabolically and phenotypically in pregnant rats. Of note, while DHT-exposed and INS-exposed

pregnant rats had decreased glucose tolerance and increased circulating TNF-α levels compared to controls, only INS-exposed pregnant rats exhibited decreased expression of insulin receptor and insulin receptor substrate mRNAs in the mesenteric fat, but not in the liver, compared to controls (Fig. 5A,B).

Our previous studies indicated that early and mid-gestational exposure to DHT and insulin and to DHT

Fig. 2. Localization and expression of HMGB1 protein in endometria collected from non-pregnant women with and without PCOS in the proliferative phase. (A) Representative immunohistochemical images of intracellular HMGB1 localization. Tissue sections were counterstained with methyl green (n = 3 per group, each from different patients). The black arrows indicate infiltrated immune cells in the endometrial gland. Negative control staining is shown in the lower panel. Tissue sections were counterstained with methyl green. Ge, glandular epithelial cells; Le, luminal epithelial cells; str, stromal cells. Scale bars are 100 μm. (B) Representative western blot from endometrial lysates from non-PCOS (control) and PCOS patients probed with antibodies against HMGB1. Data are presented as fold changes in comparison to controls (n = 6 per group, each from different patients). Values are expressed as means ± SEM. Between-group comparison was carried out by Student's t-test, and differences between the groups are reported as *P < 0.05.

(A)
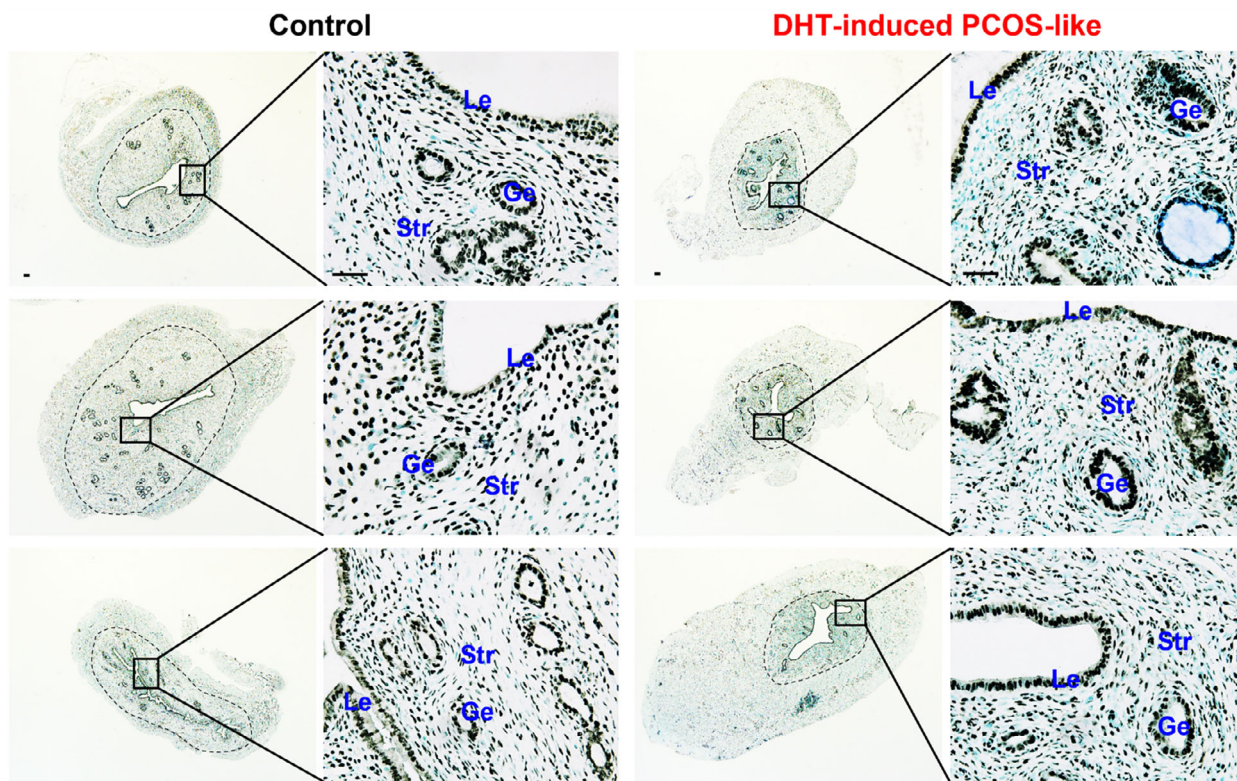
Proliferative phase

(B)
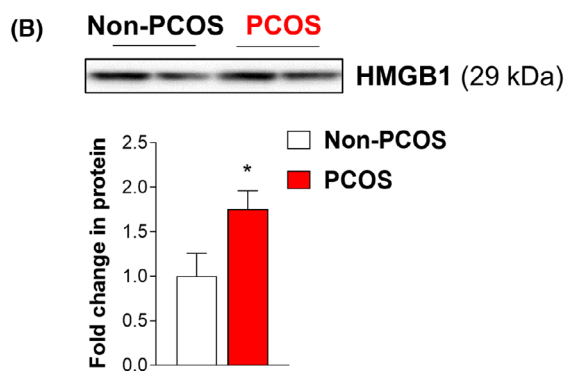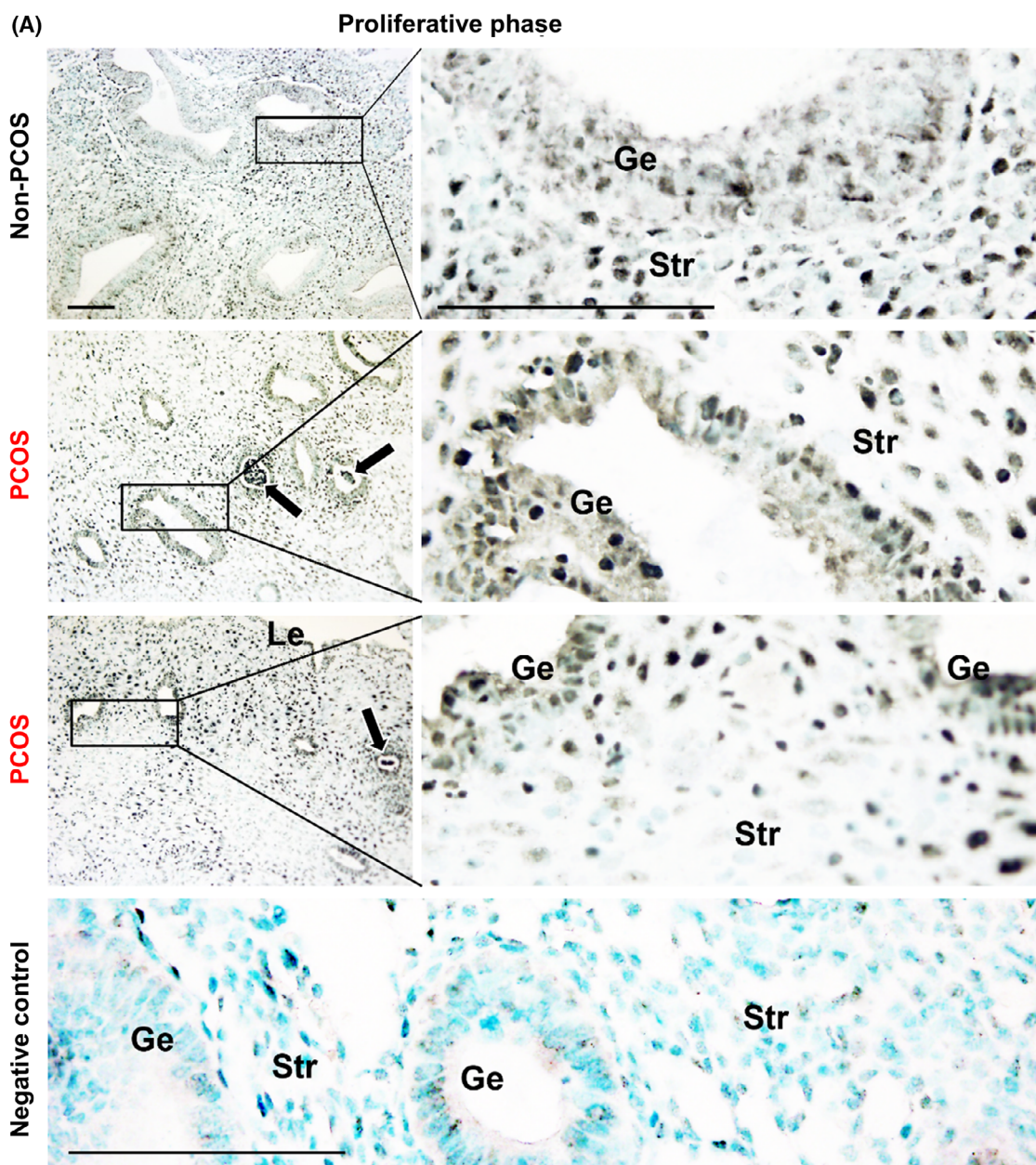
Fig. 3. Localization of HMGB1 protein in uteri collected from non-pregnant rats exposed to DHT. To establish the hyperandrogenic PCOS-like animal model, female Wistar rats (21 days old) were implanted subcutaneously with a DHT silicone tube in the nape of their neck that contained 7.5 mg DHT and that released a daily dose of 83 μg for 90 days. Control rats (the dioestrus stage) were implanted subcutaneously with the same silicone tubes but without DHT. Representative immunohistochemical images of intracellular HMGB1 localization. Tissue sections were counterstained with methyl green (n = 3 per group, each from different animals). Enhanced magnifications are shown in the right panels of each photomicrograph. Ge, glandular epithelial cells; Le, luminal epithelial cells; str, stromal cells. Scale bars are 100 μm.

alone results in implantation failure and fetal loss [40,41,48]. As expected, at GD 14.5, the uterus maintained the features of pregnancy, including the mesometrial decidua and triangle, placenta and fetus in control and INS-exposed pregnant rats, whereas the uterus contained endometrial and myometrial compartments in DHT + INS-exposed and DHT-exposed pregnant rats (Fig. 5C). Furthermore, in the uterine mucosa (the endometrium), extensive proliferation in the luminal epithelium was observed in DHT + INS-exposed and DHT-exposed pregnant rats (Fig. 5C). Physiologically, uterine stromal cell decidualization is the predominant process of uterine preparation for pregnancy, and alterations in decidualization-dependent uterine cell morphology such as decidualized stromal cells with round nuclei and pale basophilic cytoplasm are seen during early pregnancy [51]. We found the defective decidual response (referred to as clusters of fibroblast-like stromal cells and the presence of stromal cells with pyknotic and karyorrhectic nuclei) in both DHT + INS-exposed

and DHT-exposed pregnant rat uteri (Fig. 5C). These findings, corroborated by consistent observations in human endometrial stromal cells *in vitro* [52,53], indicate that *in vivo* exposure to DHT and insulin or DHT alone resulted in implantation failure and infertility in pregnant rodents [41,42] due to the compromised endometrial receptivity and stromal cell decidualization in the gravid uterus.

The regulatory patterns of uterine HMGB1 and its receptors during early and mid-pregnancy

The above results prompted us to determine whether HMGB1 and TLR 2/4 protein abundance is regulated in the gravid uterus during normal pregnancy establishment, and if so, to what extent the dynamics of uterine HMGB1, TLR 2 and TLR4 protein expression change following DHT and/or INS exposure. Western blotting analysis showed significant differences between treatments for HMGB1, TLR2 and TLR4 protein abundance
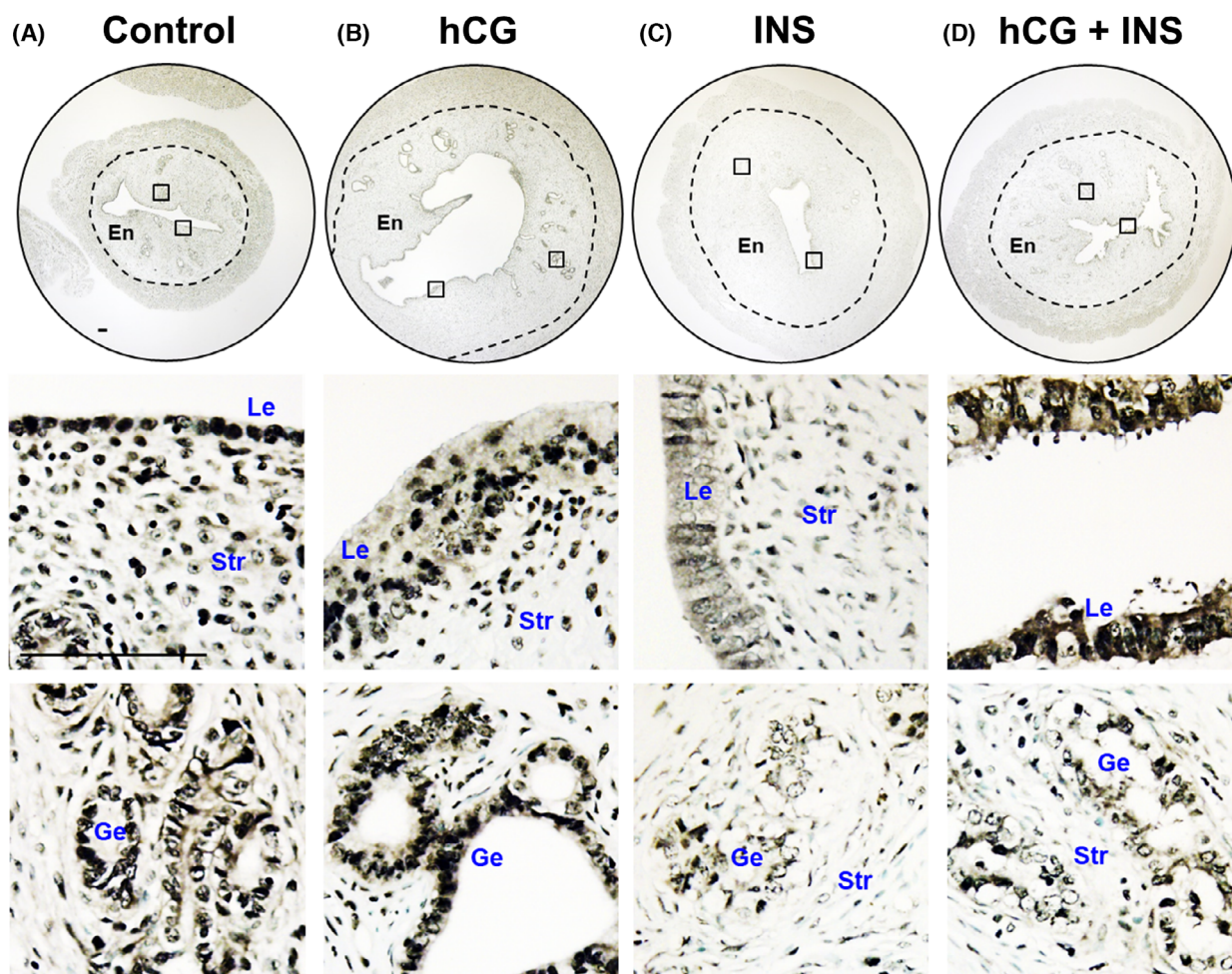
Fig. 4. Localization of HMGB1 protein in uteri collected from non-pregnant rats exposed to hCG and/or INS. Female Sprague–Dawley rats (70 days old) were randomly divided into four groups and exposed to (A) an equal volume of saline as controls; (B) 3.0 IU·day^{-1} hCG to elevate endogenous androgen levels and to induce hyperandrogenism; (C) insulin (INS), which was started at 0.5 IU·day^{-1} and gradually increased to 6.0 IU·day^{-1} between the 11th day and the 22nd day to induce hyperinsulinemia and peripheral insulin resistance; or (D) hCG plus INS to induce a combination of hyperandrogenism and hyperinsulinemia (referred as the PCOS-like rats). Animals were given twice-daily subcutaneous injections and then decapitated on the 23rd day. Representative immunohistochemical images of intracellular HMGB1 localization. Tissue sections were counterstained with methyl green (n = 3–5 per group, each from different animals). Enhanced magnifications are shown below each photomicrograph. En, endometrium; Ge, glandular epithelial cells; hCG, human chorionic gonadotropin; Le, luminal epithelial cells; str, stromal cells. Scale bars are 100 μm.

(P_{Treat} < 0.001) and between different GDs for TLR4 protein abundance (P_{GD} = 0.004; Fig. 6A). Further analysis showed that the levels of HMGB1 and TLR4 were decreased in control pregnant rats at GD 14.5 compared to those at GD 4.5, while the levels of TLR2 and TLR4 were decreased in INS-exposed pregnant rats at GD 14.5 compared to those at GD 4.5 (Fig. 6A). Of note, exposure to DHT + INS significantly affected uterine HMGB1 abundance only at GD 14.5 and not at other GDs. We found that uterine HMGB1, TLR2 and TLR4 protein abundance was increased in DHT + INS-exposed pregnant rats compared to controls. Despite TLR2 and TLR4 protein abundance being increased, no significant change in HMGB1 protein abundance was observed in DHT-exposed pregnant rats compared to controls at GD 14.5 (Fig. 6A). Pearson's correlation analysis showed a significant correlation between HMGB1 and TLR2 proteins in DHT + INS-exposed and DHT-exposed pregnant rats from GD 4.5 to GD 14.5 (Fig. 6B). We also found that uterine HMGB1 protein abundance either tended to be or was significantly correlated with TLR4 protein abundance in control and DHT + INS-exposed pregnant rats from GD 4.5 to GD 14.5 (Fig. 6B).
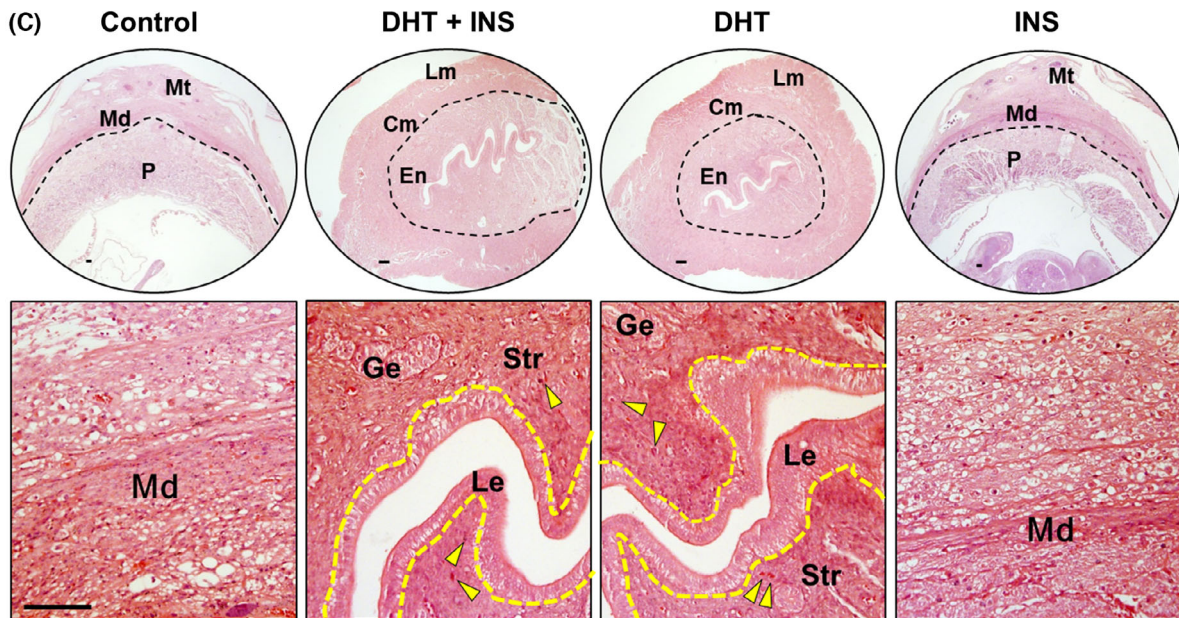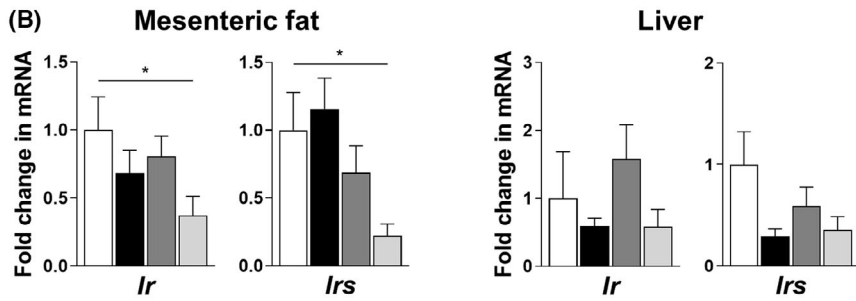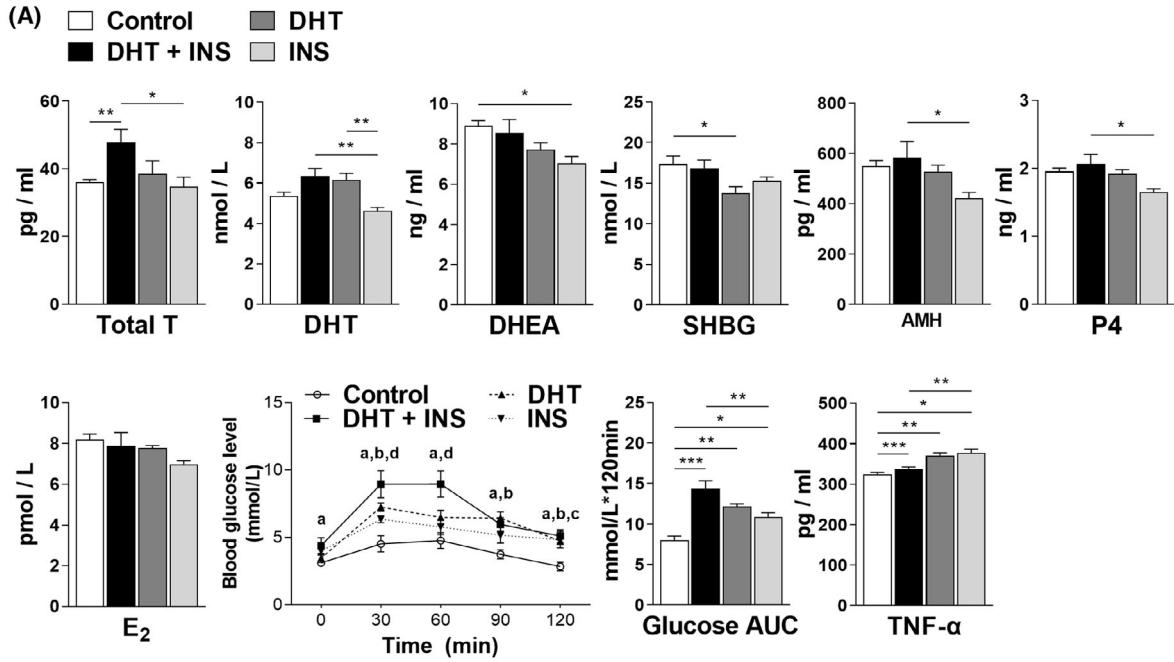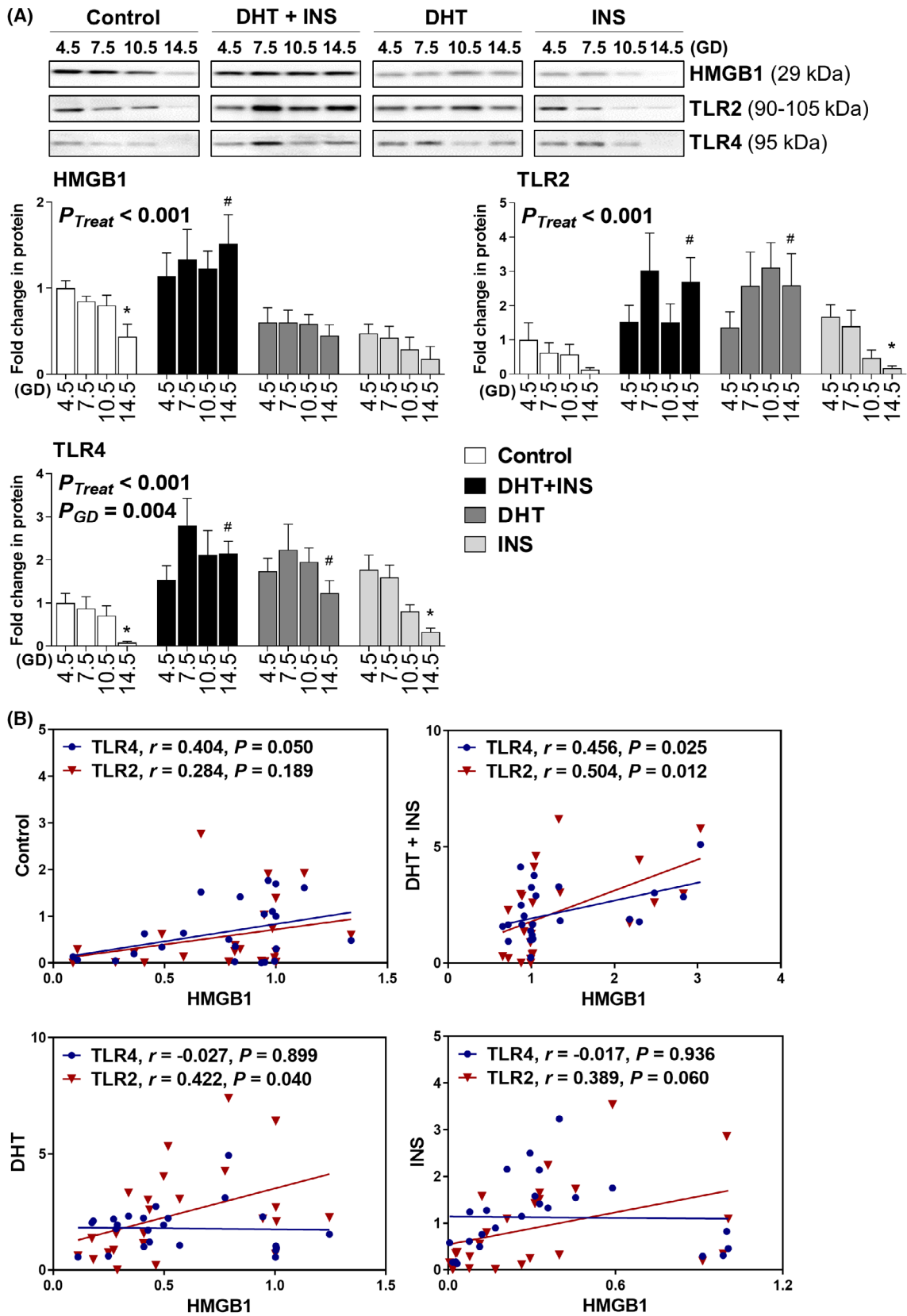
Fig. 5. Aberrant regulation of circulating hormone, glucose and cytokine levels, and insulin receptor (*Ir*)/insulin receptor substrate (*Irs*) gene expression, as well as the uterine morphology in pregnant rats exposed to DHT and/or INS at GD 14.5. (A) Comparison of circulating T, DHT, DHEA, SHGB, AMH, P4, E2, blood glucose concentrations during OGTT, area under the curve (AUC) for glucose and TNF-α in pregnant rats treated with DHT and/or INS (*n* = 6 per group, each from different animals). AUC was calculated by the formula $[0.5 \times (BG0 + BG30)/2 + 0.5 \times (BG30 + BG60)/2 + 0.5 \times (BG60 + BG90)/2 + 0.5 \times (BG90 + BG120)/2]$, where the BG terms are the blood glucose levels at 0, 30, 60, 90 and 120 min. Statistical tests are described in the Materials and methods, and differences between the groups are reported as $*P < 0.05$, $**P < 0.01$ and $***P < 0.001$. $^aP < 0.05$, control vs. DHT + INS; $^bP < 0.05$, control vs. DHT; $^cP < 0.05$, control vs. INS; $^dP < 0.05$, DHT + INS vs. INS. (B) Comparison of *Ir* and *Irs* mRNAs in the adipose tissues and livers of pregnant rats treated with DHT and/or INS (*n* = 6 per group, each from different animals). Values are expressed as means ± SEM. Between-group comparisons were carried out by either one-way ANOVA followed by Tukey's *post hoc* test or Kruskal–Wallis test, and differences between the groups are reported as $*P < 0.05$. (C) Representative histological images of gravid uteri using H&E staining in pregnant rats treated with vehicle, DHT + INS, DHT or INS at GD 14.5 (*n* = 6 per group, each from different animals). The yellow arrowheads indicate the presence of stromal cells with pyknotic and karyorrhectic nuclei. Cm, circular myometrium; En, endometrium; Ge, glandular epithelial cells; Le, luminal epithelial cells; Lm, longitudinal myometrium; Md, mesometrial decidua; Mt, mesometrial triangle; P, placental disc; str, stromal cells. Scale bars are 100 μm.

Using immunohistochemical assays, we showed that in control pregnant rats (Fig. 7A–D), HMGB1 was expressed ubiquitously in epithelial, decidual, stromal and myometrial smooth muscle cells in the gravid uterus at GD 4.5 (Fig. 7A1), GD 7.5 (Fig. 7B1) and GD 10.5 (Fig. 7C1). However, nuclear HMGB1 immunoreactivity was reduced in the mesometrial decidua and triangle compartments at GD 14.5 (Fig. 7D1). Of note, in addition to its nuclear localization, cytoplasmic HMGB1 immunoreactivity was also detected in control uteri with both haemorrhagic and resorbed fetuses (Fig. 7E,F). We also found a similar expression of cellular HMGB1 immunoreactivity over the course of gestation between control (Fig. 7A1–D1) and INS-exposed pregnant rat uteri (Fig. 8A1–D1). In contrast, immunostaining for HMGB1 was consistently present in all cell types of the gravid uterus of DHT + INS-exposed (Fig. 9A–D) and DHT-exposed pregnant rats (Fig. 9E–H) regardless of the GD. These findings indicate that the co-occurrence of hyperandrogenism and insulin resistance plays a key role in abnormal uterine HMGB1 protein abundance and corresponding TLR2 and TLR4 protein abundance during pregnancy.

AR-dependent up-regulation of HMGB1, TLR2 and TLR4 expression is associated with the enhancement of gravid uterine inflammation

To evaluate the role of the androgen–AR axis in regulating HMGB1 protein expression and the molecular events related to uterine inflammation, pregnant control and DHT + INS-exposed rats were treated chronically with the AR antagonist flutamide. Hyperandrogenism and insulin resistance (as features of PCOS) in pregnant rats are suppressed by flutamide treatment [48], and we observed significantly decreased protein abundance of AR, HMGB1, TLR2 and TLR4

in DHT + INS-exposed pregnant rats treated with flutamide (with viable fetuses) compared to those without flutamide treatment (Fig. 10A). Hyperandrogenism has been implicated as a key regulatory factor for PCOS-related inflammation, which is likely due to activation of the NFκB signalling pathway [54]. As shown in Fig. 10B, chronic treatment with flutamide normalized DHT + INS-induced alterations of cyclooxygenase 2 (Cox2, an enzyme for inflammatory mediator prostaglandin synthesis, which is required for stromal decidualization), an inhibitor of nuclear factor κB alpha (IkBα), NFκB p65, phosphorylated signal transducer and activator of transcription 3 (p-Stat3) and Stat3 protein levels, as well as the ratio of p-Stat3 to Stat3 (an indicator of shifting the balance from pro- to anti-inflammatory responses during early pregnancy). In addition, flutamide treatment increased Ikappa B kinase alpha (IKKα) and IKKβ protein levels (Fig. 10B) and decreased cytokine IL-6 protein levels (Fig. 10C) in DHT + INS-exposed pregnant rats (with fetuses) compared to those without flutamide treatment. There was no effect of flutamide on AR, HMGB1, TLR2, TLR4, Cox2, IKKβ, IkBα, NFκB p65, p-Stat3, Stat3 or IL-6 protein abundance in pregnant control rats (Fig. 10A–C). Although HMGB1 is a nuclear protein, it can be translocated to the cytoplasm to modulate intracellular signalling and eventually is secreted outside the cells [23,27]. To investigate the link between the activation of the hyperandrogenism/AR axis and circulating HMGB1 levels, we performed an ELISA for determining the circulating HMGB1 levels in pregnant rats exposed to DHT and insulin. As shown in Fig. 10D, the circulating HMGB1 levels were higher in DHT + INS-exposed pregnant rats than in controls despite uncertainty in the cellular origin of HMGB1. Moreover, chronic treatment with flutamide normalized
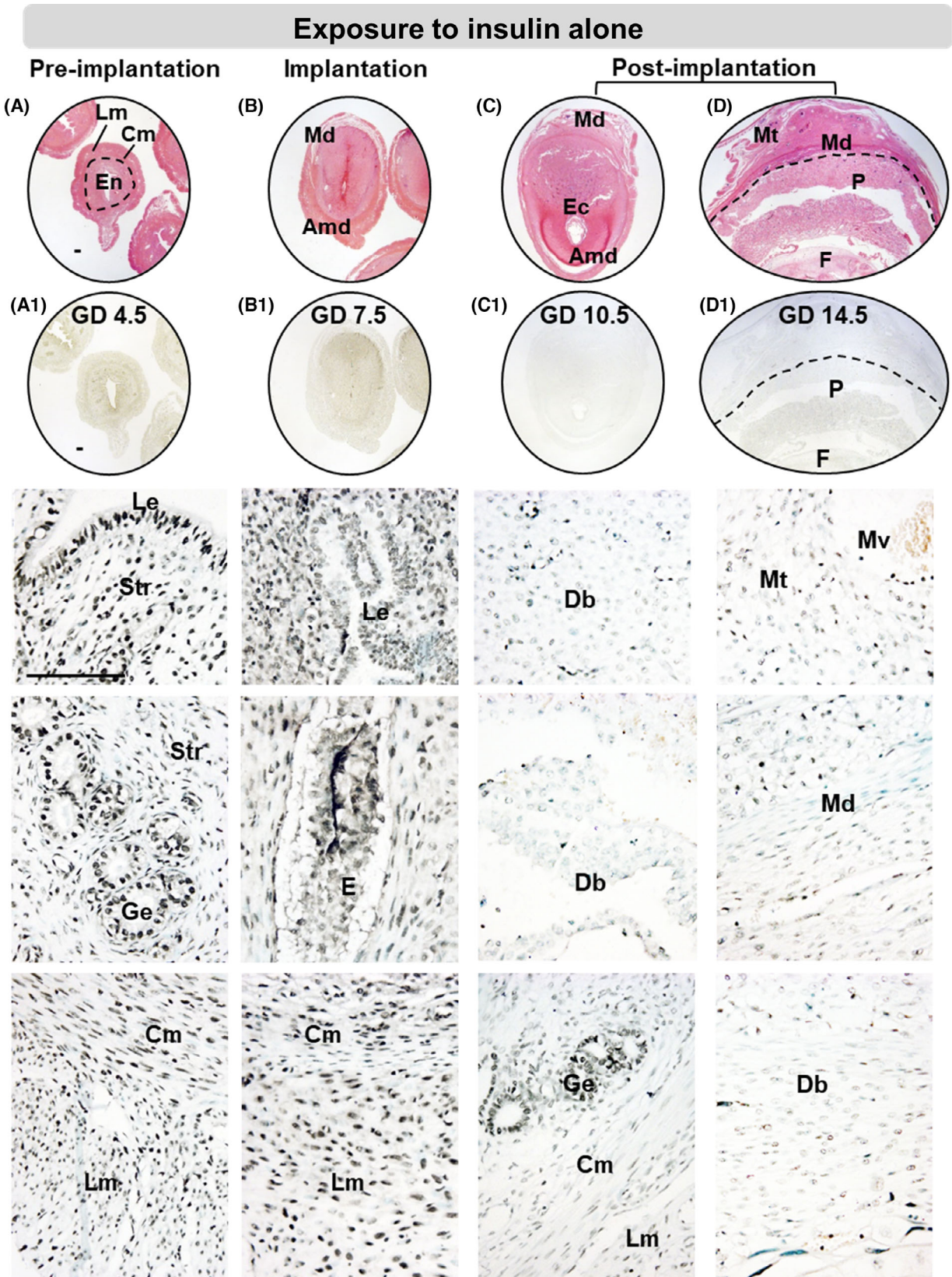
Fig. 6. Gestational age-dependent regulation of and correlation among HMGB1, TLR2 and TLR4 proteins in uteri collected from pregnant rats exposed to DHT and/or INS from GD 4.5 to GD 14.5. (A) Representative western blot from uterine lysates from pregnant rats exposed to vehicle (control), DHT + INS, DHT or INS probed with anti-HMGB1, anti-TLR2 and anti-TLR4 antibodies. In all plots, the data are presented as the fold change in comparison to control pregnant rats (GD 4.5 values, $n = 6$ per group, each from different animals). Values are expressed as means ± SEM. Between-group comparisons were carried out by two-way ANOVA followed by pair-wise Tukey's *post hoc* test, and the main effects of GD and/or hormonal treatment are referred to as P_{GD}, P_{Treat} and $P_{GD:Treat}$ respectively (see 'Results' section for details). * Significantly different compared to the respective treatment at GD 4.5 ($P < 0.05$); # Significantly different compared to the control group at GD14.5 ($P < 0.05$). (B) Pearson's correlation analysis of HMGB1, TLR2 and TLR4 protein expression in the gravid uterus. The scatterplots illustrate the relationship among HMGB1, TLR2 and TLR4, and Pearson's correlation coefficients (*r*) and *P*-values are shown. INS, insulin.

Fig. 7. Localization of HMGB1 protein in uteri collected from control pregnant rats from GD 4.5 to GD 14.5. (A—D) Representative histological images of gravid uteri by H&E staining. (A1—D1) Representative immunohistochemical images of intracellular HMGB1 localization. Tissue sections were counterstained with methyl green ($n = 6$ per group, each from different animals). Enhanced magnifications are shown below each photomicrograph. (E, F) Representative gross morphological appearance of conceptuses within the uterine conditions at GD 14.5 collected from control pregnant rats ($n = 6$ per group, each from different animals). Representative immunohistochemical images of HMGB1 counterstained with methyl green with their enhanced magnifications are shown to the right. Black arrowhead indicates fetal death (as identified by its haemorrhagic appearance compared to normal embryos), the black arrow indicates the resorbed fetus (as identified by its small size and necrotic death compared to normal embryos) and the red arrow indicates the apoptotic embryo. GD, gestational day; En, endometrium, Cm, circular myometrium; Lm, longitudinal myometrium; Md, mesometrial decidua; Amd, antimesometrial decidua; Ac, amniotic cavity containing the fetus; Amd, antimesometrial decidua; Anm, amorphous necrotic mass; Cm, circular myometrium; Db, decidual basalis; E, embryo; Ec, ectoplacental cone; En, endometrium; F, fetus; GD, gestational day; Gd, glycogenic decidua; Ge, glandular epithelial cells; Le, luminal epithelial cells; Lm, longitudinal myometrium; Md, mesometrial decidua; Mt, mesometrial triangle; Mv, maternal vessel; P, placenta; Pdz, primary decidual zone; Str, stromal cells. Scale bars are 100 μm.

Fig. 8. Localization of HMGB1 protein in uteri collected from INS-exposed pregnant rats from GD 4.5 to GD 14.5. (A—D) Representative histological images of gravid uteri using H&E staining. (A1—D1) Representative immunohistochemical images of intracellular HMGB1 localization. Tissue sections were counterstained with methyl green (*n* = 6 per group, each from different animals). Enhanced magnifications are shown below each photomicrograph. Amd, antimesometrial decidua; Cm, circular myometrium; Db, decidual basalis; E, embryo; Ec, ectoplacental cone; En, endometrium; F, fetus; GD, gestational day; Ge, glandular epithelial cells; Le, luminal epithelial cells; Lm, longitudinal myometrium; Md, mesometrial decidua; Mt, mesometrial triangle; Mv, maternal vessel; P, placenta; Str, stromal cells. Scale bars are 100 μm.
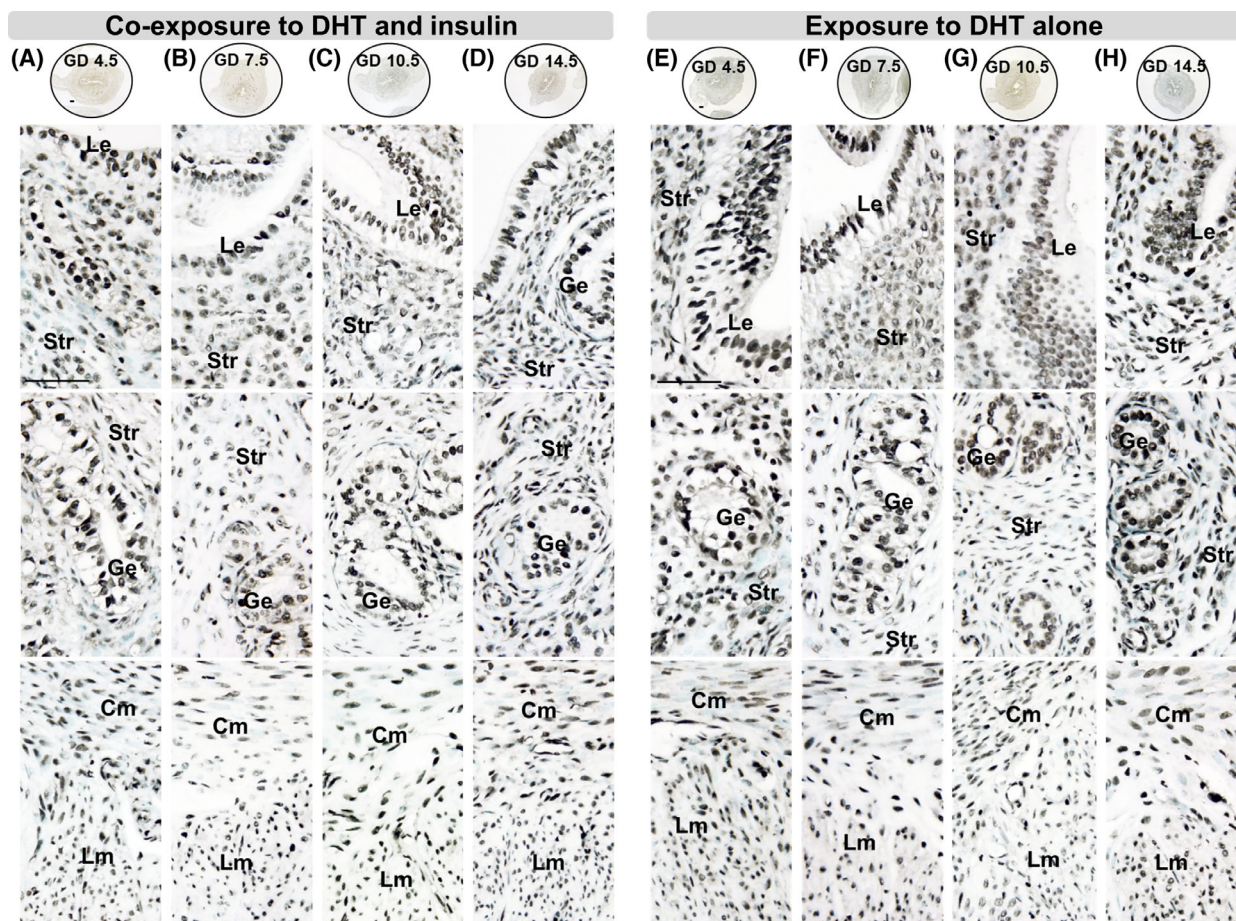

Fig. 9. Localization of HMGB1 protein in uteri collected from DHT + INS-exposed and DHT-exposed pregnant rats from GD 4.5 to GD 14.5. (A—H) Representative immunohistochemical images of intracellular HMGB1 localization. Tissue sections were counterstained with methyl green (*n* = 6 per group, each from different animals). Enhanced magnifications are shown below each photomicrograph. Cm, circular myometrium; GD, gestational day; Ge, glandular epithelial cells; Le, luminal epithelial cells; Lm, longitudinal myometrium; Str, stromal cells. Scale bars are 100 μm.

DHT + INS-induced elevation of circulating HMGB1 levels. These findings indicate that the activation of endogenous AR leads to up-regulated HMGB1 expression and systemic/uterine inflammation under PCOS conditions. Androgens can directly activate and regulate Erk1/2, which are the downstream kinases of mitogen-activated protein kinases, *in vivo* [55]. We showed that treatment with flutamide decreased p-Erk1/2 protein abundance and tended to significantly decrease the ratio of p-Erk1/2 to Erk1/2 (Fig. 10E).

Furthermore, western blot analysis demonstrated that uterine progesterone receptor A isoform (PRA) protein abundance and the ratio of PRA-to-progesterone receptor B isoform (PRB) were increased in DHT + INS-exposed pregnant rats compared to controls, whereas treatment with flutamide decreased uterine PRA protein abundance and decreased the ratio of PRA to PRB (Fig. 10F). These findings suggest that an interaction between AR and PR is involved in PCOS-induced gravid uterine inflammation.
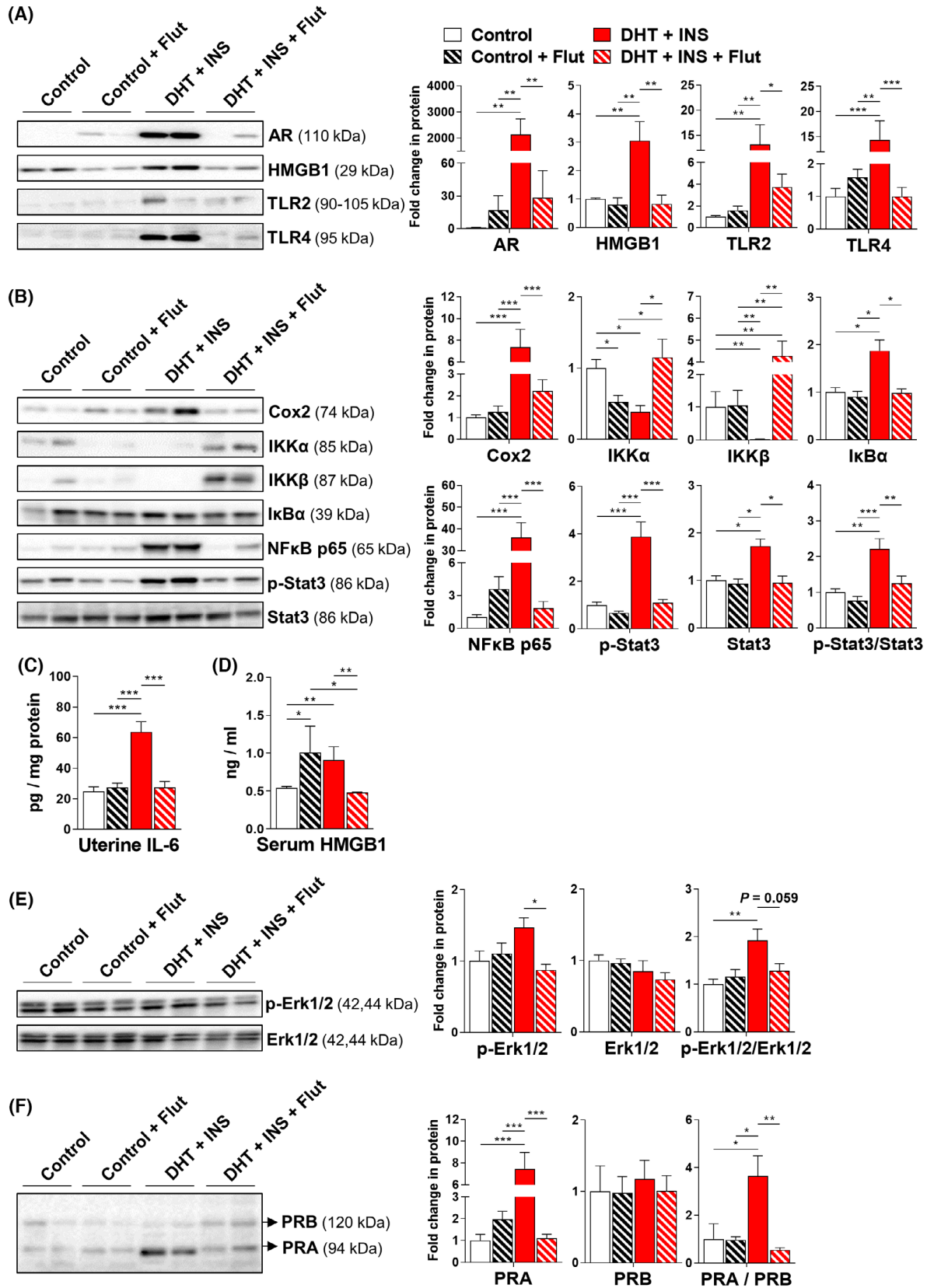
Fig. 10. The impact of flutamide on uterine AR, HMGB1, TLR2 and TLR4 protein levels, NFkB signalling activation, pro-/anti-inflammatory protein levels, Erk1/2 phosphorylation and PR protein levels in control and DHT + INS-exposed pregnant rats at GD 14.5. (A, B, E and F) Representative western blot from uterine lysates from control and DHT + INS-exposed pregnant rats treated with flutamide (with fetuses) probed with antibodies against AR, HMGB1, TLR2 and TLR4 (A), Cox2, NFκB signalling molecules and Stat3 (B), Erk1/2 (E) and PRA/PRB (F). (C, D) Uterine IL-6 and serum HMGB1 levels were determined by ELISA. In all plots, data are presented as fold changes in comparison to controls (GD 14.5 values, $n = 6$ per group, each from different animals). Values are expressed as means $\pm$ SEM. Between-group comparisons were carried out by either one-way ANOVA followed by Tukey's *post hoc* test or Kruskal–Wallis test, and differences between the groups are reported as $*P < 0.05$, $**P < 0.01$ and $***P < 0.001$. Flut, flutamide; INS, insulin.

Long-term exposure to DHT alone fails to alter HMGB1, TLR2 or TLR4 protein levels in the gravid uterus

Given the critical role of hyperandrogenism in regulating uterine inflammation [6], we examined whether long-term exposure to DHT affects HMGB1 and TLR2/4 protein expression and inflammation in the gravid uterus. As shown in Fig. 11, long-term exposure to DHT increased uterine AR protein abundance (Fig. 11A) and, in particular, increased nuclear AR immunoreactivity in luminal and glandular uterine epithelial cells (Fig. 11B) in pregnant control rats at GD 14.5 compared to those at GD 0.5. Further, co-immunoprecipitation and western blotting experiments demonstrated that endogenous AR interacts directly with HMGB1 in the gravid uterus. However, this interaction was not changed when the gravid uterus was exposed to DHT (Fig. 11C). Despite no significant changes in IKKβ, IkBα, NFκB p65, p-Stat3 and Stat3 protein expression, DHT exposure increased COX2 and IL-6 protein levels and decreased IKKα protein levels in the gravid uterus (Fig. 11D,E). If HMGB1/TLR2/TLR4 signalling is required for hyperandrogenic regulation of uterine inflammation, then exogenous DHT exposure should be able to alter uterine HMGB1 and TLR2/4 protein expression during pregnancy. However, we observed no effect of supraphysiological DHT exposure on uterine HMGB1, TLR2, or TLR4 protein expression in pregnant control rats between GD 0.5 and GD 14.5 (Fig. 11A). Furthermore, we observed that similar to co-exposure to DHT and insulin (Fig. 10E) exposure to DHT alone increased p-Erk1/2 protein abundance and increased the ratio of p-Erk1/2 to Erk1/2 (Fig. 11F), thus suggesting a possible mechanism for hyperandrogenism-induced uterine inflammation through activation of the Erk1/2 mitogen-activated protein kinase pathway during pregnancy. Although the interaction between HMGB1 and TLRs can promote inflammation through activation of the NFκB signalling pathway [22,23], these findings indicate that hyperandrogenism-enhanced gravid uterine inflammation does not fully depend on changes in HMGB1 and TLR2/4 protein expression during pregnancy.

Acute exposure to LPS causes fetal loss and disrupted gravid uterine morphology

We and others have previously shown that pregnant rodents under conditions of hyperandrogenism (resulting from chronic exposure to DHT or testosterone) exhibit elevated uterine AR expression and increased fetal loss [40–42]. Moreover, maternal exposure to LPS results in implantation failure and fetal demise through the promotion of abnormal maternal inflammation [56,57]. To test whether the activation of androgen–AR signalling is a functional requirement for HMGB1/TLR4 protein elevation and maternal inflammation-mediated pregnancy loss, we first determined whether mid-gestational exposure to LPS could detrimentally affect embryo implantation and fetal survival similarly to exposure to DHT. Pregnant rats at GD 7.5 were treated with a single dose of LPS and the gravid uterine tissues were harvested at GD 14.5. We observed that LPS-exposed pregnant rats had a disrupted implantation process, with a reduced number of viable fetuses and increased fetal loss rate compared to controls (Fig. 12A). When examined by H&E staining, the gravid uterus of the LPS-exposed pregnant rats had more haemorrhages and more fibrin deposition in the lumen of vessels than controls (Fig. 12B), which was in accordance with previous studies [57,58]. In line with the findings in control uteri with resorbed fetuses (Fig. 7F), cytoplasmic and nuclear HMGB1 and NFκB p65 immunoreactivity was detected in the LPS-exposed gravid uterus with resorbed fetuses (Fig. 13). The cleaved caspase-3 protein expression was absent in LPS-exposed uteri with viable fetuses (Fig. 14). However, pregnant rats exposed to LPS showed hardly any increase in circulating levels of hormones, including all androgens (total T, A4 and DHT), AMH, P4 and E2 compared to control pregnant rats (Fig. 12C). These findings indicate that the androgen-independent elevation of uterine HMGB1 protein expression is related to LPS-induced maternal inflammation-mediated fetal loss.
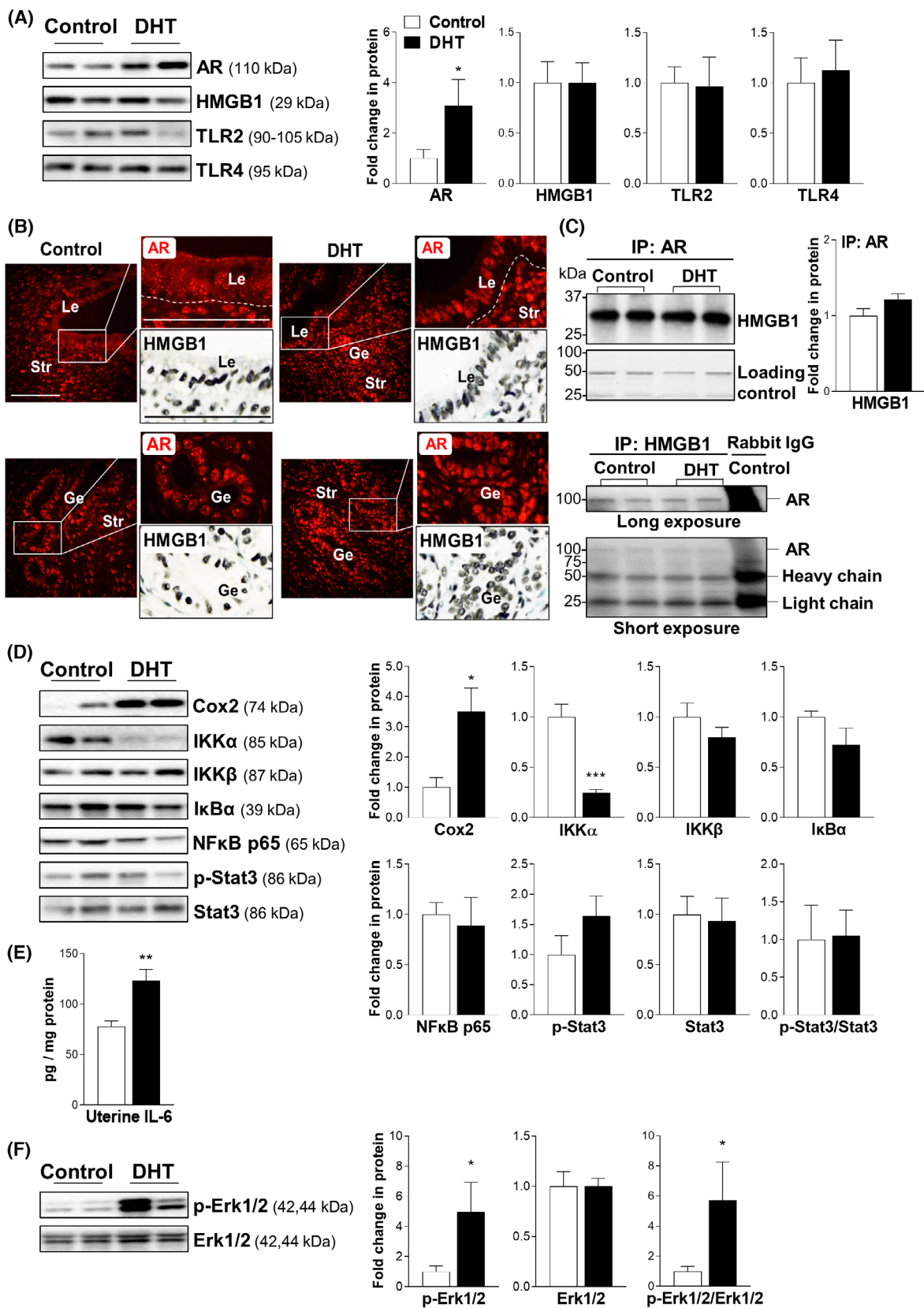
Fig. 11. The impact of DHT exposure on uterine AR, HMGB1, TLR2 and TLR4 protein levels, NFκB signalling activation, pro-/anti-inflammatory protein levels, Erk1/2 phosphorylation protein levels and HMGB1 and AR interactions. (A) Representative western blot from uterine lysates from control pregnant rats (GD 0.5) chronically exposed to DHT (GD 14.5) probed with antibodies against AR, HMGB1, TLR2 and TLR4. (B) Representative immunohistochemical images of AR and HMGB1 counterstained with methyl green (n = 3 tissue replicates from control and DHT-exposed rats). Enhanced magnifications are shown in the right panels of each photomicrograph. Ge, glandular epithelial cells; Le, luminal epithelial cells; str, stromal cells. Scale bars represent 100 μm. (C) *In vivo* co-immunoprecipitation of HMGB1 with AR. Uterine tissues were immunoprecipitated (IP) with anti-AR or anti-HMGB1 antibody and then probed with anti-HMGB1 or anti-AR antibody and processed for western blotting. The rabbit IgG isotype was used as the control. (D) Representative western blot from uterine lysates from control pregnant rats (GD 0.5) chronically exposed to DHT (GD 14.5) probed with antibodies against Cox2, NFκB signalling molecules and Stat3. (E) Uterine IL-6 levels were determined by ELISA. (F) Representative western blot from uterine lysates from control pregnant rats (GD 0.5) chronically exposed to DHT (GD 14.5) probed with antibodies against Erk1/2. In all plots, data are presented as fold changes in comparison to controls (GD 0.5 values, n = 6 per group, each from different animals). Values are expressed as means ± SEM. Between-group comparisons were carried out by either Student's *t*-test or Mann–Whitney *U*-test, and differences between the groups are reported as *$P < 0.05$, **$P < 0.01$ and ***$P < 0.001$.

AR-independent down-regulation of HMGB1 and TLR4 expression is associated with the suppression of inflammation in the gravid uterus with viable fetuses

Next, consistent with our observations from control pregnant rats at GD 7.5 and GD 14.5 (Fig. 7B1,D1), a similar pattern of HMGB1 immunoreactivity was found in control pregnant rats at the same respective GD (Fig. 12D). In addition, LPS-exposed pregnant rat uteri with viable fetuses displayed low HMGB1 immunoreactivity in the mesometrial decidua and triangle compartments similar to GD-matched control rat uteri (Fig. 12D). Uterine AR protein expression was undetectable in control pregnant rats at GD 14.5, consistent with a previous study [48], and acute exposure to LPS did not alter AR protein expression in uteri with viable fetuses (Fig. 15A). We observed that decreased HMGB1 and TLR4 protein levels were associated with the absence of AR protein expression in both control and LPS-exposed pregnant rat uteri with viable fetuses (Fig. 15A). Further, no statistically significant changes were seen in TLR2, IKKα, IkBα, p-Stat3, Stat3 or IL-6 protein expression or in circulating HMBG1 levels, while lower Cox2 and NFκB p65 protein levels and higher IKKβ protein levels were found in LPS-exposed pregnant rat uteri with viable fetuses compared to GD-matched control rat uteri (Fig. 15). These findings indicate that AR-independent regulation of uterine HMGB1 and TLR4 protein expression is linked to LPS-induced maternal inflammation, which contributes to pregnancy loss.

Discussion

Hyperandrogenism and insulin resistance play central roles in the pathophysiology of PCOS [1,4] and have a strong negative impact on pregnancy outcomes [3,5,6]. Presently, no experimental studies have addressed the impact of maternal PCOS stimuli on regulating the protein expression of HMGB1, a modulator of embryo implantation competence [28,30,31], and its candidate receptors TLR2/4 in association with uterine inflammation during pregnancy. The findings reported here support the notion that either a direct or indirect effect of AR activation is responsible for the elevation of HMGB1, TLR2 and TLR4 proteins and the enhancement of gravid uterine inflammation and that higher uterine HMGB1 protein expression is associated with aberrant inflammation-induced fetal loss.

Successful pregnancy requires intrauterine inflammation homeostasis [8,9], whereas aberrant intrauterine inflammation is an important contributor to implantation failure and defects and to repeated miscarriages [10]. Of note, systemic low-grade chronic inflammation and hyperandrogenism co-exist in PCOS patients after pregnancy [5], and even after restoring ovulation PCOS patients still exhibit a higher rate of implantation failure and early pregnancy loss [11]. These clinical data indicate that the disturbance of inflammation homeostasis might cause uterine health to deteriorate, and subsequently lead to poor pregnancy outcomes in pregnant women with PCOS. Findings from preclinical and clinical observational studies indicate that *in vivo* and *in vitro* exposure to hyperandrogenism can directly damage endometrial receptivity and decidualization and can disrupt embryonic implantation in humans [59] and rodents [41,42,60], which leads to increased rates of pregnancy loss [40,41]. Androgen responsiveness in the endometrium is mostly if not completely mediated by the AR, which functions primarily as a nuclear receptor in regulating genomic activity [61]. Our previous study showed that uterine AR protein expression is significantly decreased during normal pregnancy, whereas the hyperandrogenic stimulation seen in PCOS induces AR protein abundance in the gravid uterus [48]. Our current data indicate
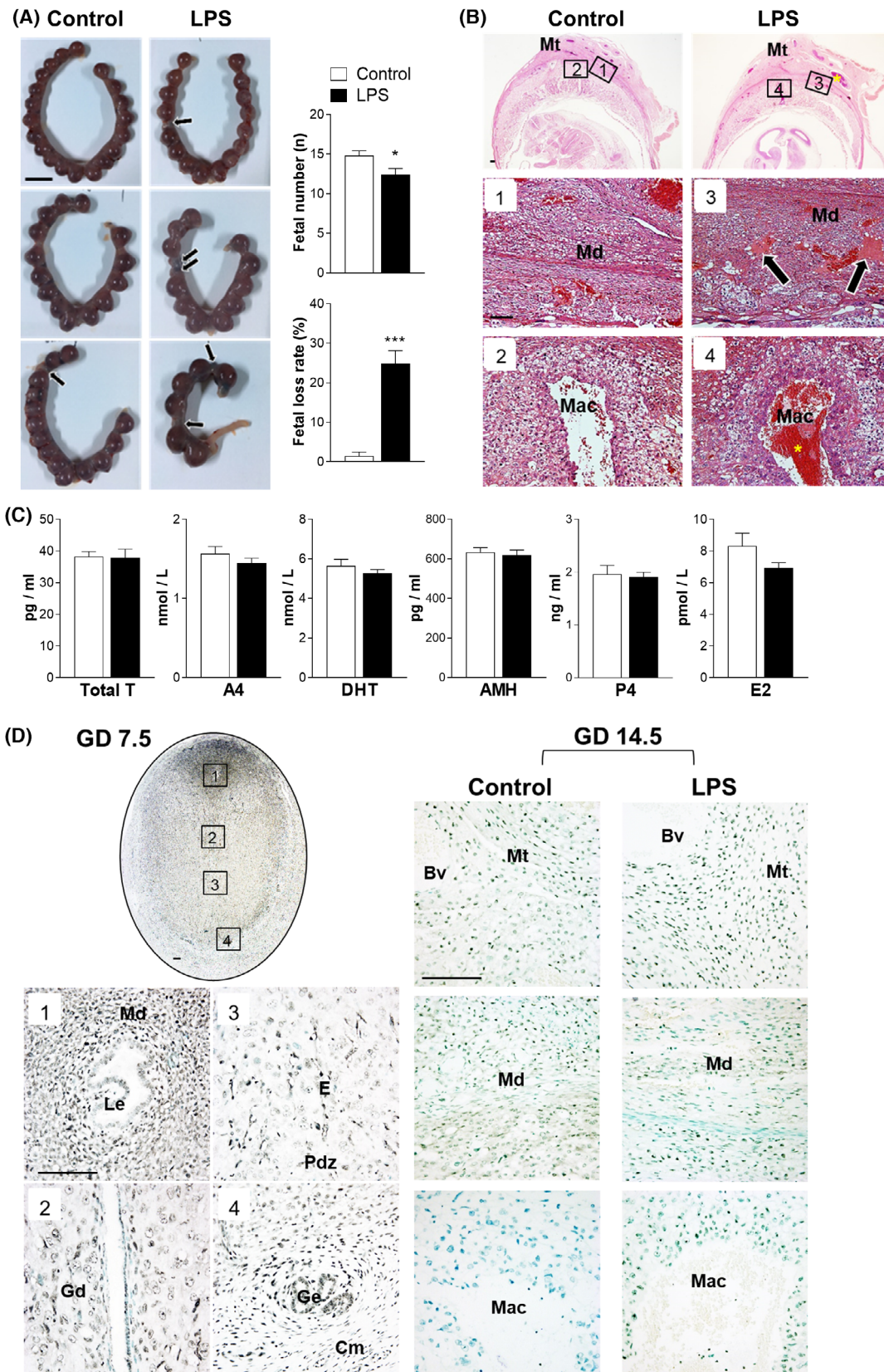
Fig. 12. The impact of LPS on pregnancy outcome, steroid hormone levels and uterine HMGB1 immunoreactivity in control pregnant rats at GD 14.5. (A) Representative gross morphological appearance of conceptuses within the uterine conditions at GD 14.5 collected from control pregnant rats exposed to saline and LPS on GD 7.5. Black arrows indicate the resorbed fetuses (as identified by their small size and necrotic death compared to normal embryos). Scale bars are 1 cm. The fetal loss rate was calculated as: Average % = non-viable fetuses/total fetuses × 100 (n = 10 per group, each from different animals). Values are expressed as means ± SEM. Between-group comparisons were carried out by Student's t-test, and differences between the groups are reported as *$P < 0.05$ and ***$P < 0.001$. (B) Representative histological images of gravid uteri using H&E staining. Images are representative of six tissue replicates from different animals, and enhanced magnifications are shown below each photomicrograph. (C) Comparison of circulating T, A4, DHT, AMH, P4 and E2 levels (n = 10 per group, each from different animals). Values are expressed as means ± SEM. Between-group comparisons were carried out by Student's t-test, and no significant difference between control and LPS-exposed pregnant rats was found. (D) Representative immunohistochemical image of HMGB1 intracellular localization. Tissue sections were counterstained with methyl green (n = 6 per group, each from different animals). Cm, circular myometrium; E, embryo; Gd, glycogenic decidua; Ge, glandular epithelial cells; Le, luminal epithelial cells; mac, maternal arterial canal (which is lined by canal trophoblast giant cells and surrounded by the spongiotrophoblast and glycogen trophoblast cells); Md, maternal decidua; Mt, mesometrial triangle; Pdz, primary decidual zone. Scale bars are 100 μm.

that the pattern of HMGB1 protein expression is mirrored by AR protein activation in the gravid uterus during normal and PCOS-like pregnancies. Because hyperandrogenism-induced AR activation has been accepted as a hallmark of uterine defects and adverse pregnancy outcomes in PCOS patients [53,62] and PCOS-like animals [42,48], and because the sustained chronic inflammation is correlated with pregnancy loss [9] in PCOS patients [11], modulation of the androgen–AR signalling axis has been considered to be an important checkpoint for identifying its downstream targets in association with disrupted inflammatory mechanisms in the gravid uterus. In this study, we show that in addition to decreased AR protein abundance (this study and [48]) and increased fetal survival in pregnant PCOS-like rats [48], treatment with the AR antagonist flutamide also decreased HMGB1, TLR2, TLR4 and NFκB p65 protein levels in the gravid uterus with viable fetuses. It has been reported that compared to women without PCOS, the levels of HMGB1 mRNA and protein are significantly increased in both ovarian granulosa cells [33–36], endometrium (in this study), follicular fluid [35] and serum [36–39] in women with PCOS. While the actions of HMGB1-induced inflammation are mediated by binding to TLRs [22,23], we show here that uterine HMGB1 and TLR2/4 protein levels are positively correlated with each other in pregnant PCOS-like rats. Our recent studies of human subjects showed that TLR4/NFκB signalling constitutes an important mechanism for regulating hyperandrogenism-driven cytokine synthesis and abnormal inflammation in the endometrium of women with PCOS [15]. Therefore, it seems likely that inhibition of nuclear AR protein elevation directly attenuates HMGB1 binding to TLR2 and TLR4 and disrupts the interaction between HMGB1 and NFκB, thus diminishing the inflammatory responses in the gravid uterus. Interestingly, treatment with flutamide has been shown

to increase the likelihood of childbirth in PCOS patients after spontaneous conception [62]. Consistent with a previous animal study [48], our findings suggest that the AR–antagonist complex suppresses uterine AR activation at least in part by inhibiting HMGB1/TLR2/TLR4 signalling, which prevents abnormal uterine inflammation and promotes sustained uterine functionality for successful pregnancy under the conditions of PCOS (Fig. 16).

HMGB1 protein has been shown to increase AR's DNA binding and transcriptional activity *in vitro* [63,64]. In our current *in vivo* study, we confirmed the previous observation that HMGB1 directly interacts with AR [64]. However, our findings are the first, to our knowledge, to demonstrate that in the uterus, the expression of HMGB1 protein and its interaction with AR is independent of hyperandrogenic stimulation. We and others have demonstrated that *in vivo* and *in vitro* exposure to DHT can increase uterine AR protein expression [48] and promote its interaction with other nuclear proteins such as melanoma antigen A11 [53] and nuclear factor erythroid 2-related factor 2 [21]. While our study does not preclude the possibility that short-term exposure to androgens may also regulate HMGB1 protein expression and interaction with AR in the uterus, the precise mechanism underlying the androgen-independent crosstalk between HMGB1 and AR in the uterus *in vivo* appears to be more complex than we originally thought.

The causes of PCOS-related HMGB1-regulated decidual inflammation are yet to be fully understood. As suggested by pre-clinical and clinical studies, insulin resistance can have adverse impacts on PCOS-related changes in uterine function through abnormal regulation of the insulin–insulin receptor signal transduction pathway [45,65,66]. For instance, phosphorylation of insulin receptor substrates, which leads to the phosphorylation of Akt and NFκB in the cytoplasm and
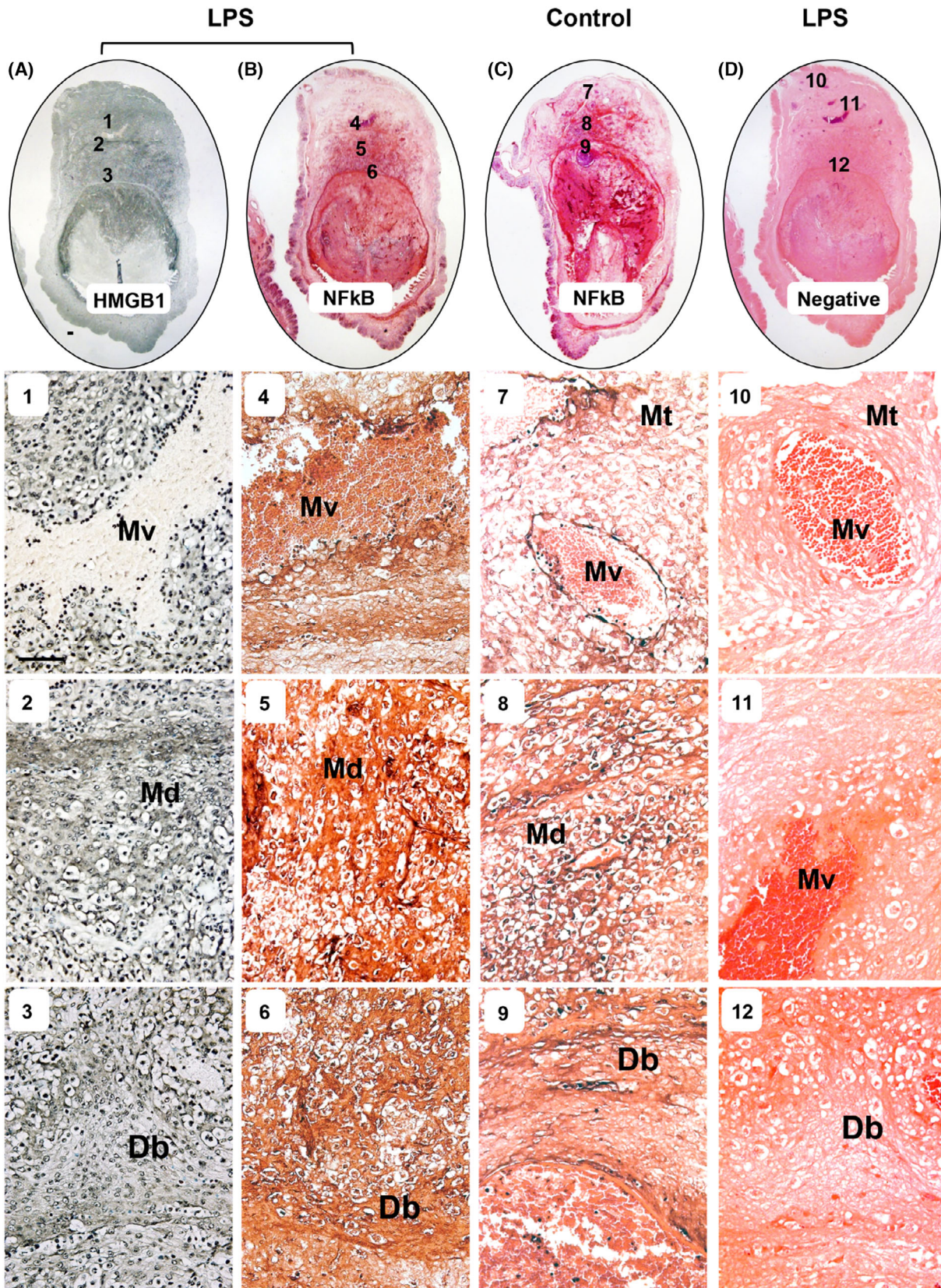
Fig. 13. Localization of HMGB1 and NFκB p65 protein in uteri with resorbed fetuses collected from control and LPS-exposed pregnant rats at GD 14.5. (A) Representative immunohistochemical images of intracellular HMGB1 localization (n = 3 per group, each from different animals). (B, C) Representative immunohistochemical images of intracellular NFκB p65 localization (n = 3 per group, each from different animals) in parallel with negative controls (D). Tissue sections were counterstained with methyl green (A) and eosin (B–D). Enhanced magnifications are shown below each photomicrograph. Db, decidual basalis; Md, mesometrial decidua; Mt, mesometrial triangle; Mv, maternal vessel. Scale bars are 100 μm.

further activation in the nucleus, is associated with an increased systemic and uterine inflammatory state (i.e. increased IL-6 gene and protein expression) in PCOS patients [15,67–70] and PCOS-like rodents [18,41,47]. While the extra-nuclear function of HMGB1 has been implicated in triggering and modulating inflammatory cascades [26,27], our findings demonstrate that HMGB1 immunoreactivity accumulates in the cytoplasm of luminal epithelial cells but not in glandular epithelial and stromal cells in the non-pregnant rat uterus exposed chronically to insulin. Interestingly, positive HMGB1 immunoreactivity was also observed in the cytoplasm of glandular epithelial cells in the PCOS endometrium. While embryo implantation proceeds from the initial attachment of the embryo to the uterine luminal epithelial cells [9], and long-term exposure to insulin induces uterine insulin resistance [45], the cell type-specific regulation of HMGB1's
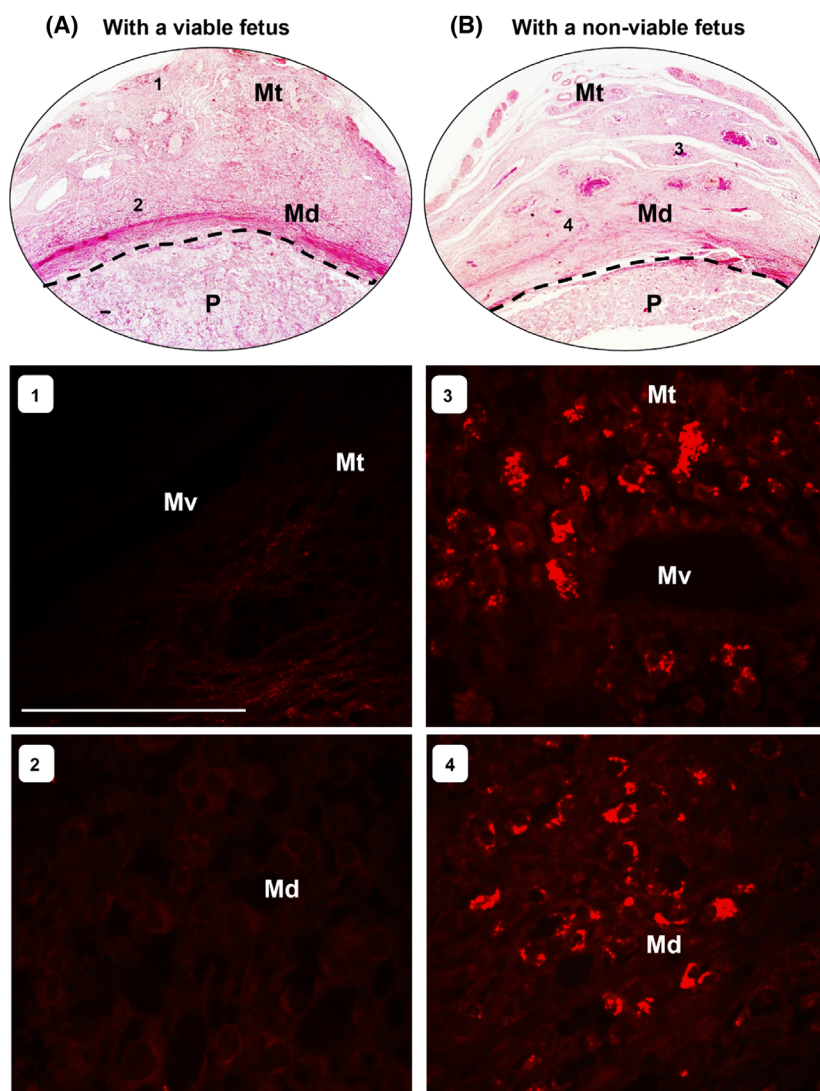

Fig. 14. Localization of cleaved caspase-3 protein in uteri with viable and non-viable fetuses collected from LPS-exposed pregnant rats at GD 14.5. (A, B) Representative histological images of gravid uteri using H&E staining (upper panel, n = 3 per group, each from different animals) and enhanced magnifications of immunofluorescence images of cleaved caspase-3 (middle and lower panels, n = 5 per group, each from different animals). Md, mesometrial decidua; Mt, mesometrial triangle; Mv, maternal vessel; P, placenta. Scale bars are 100 μm.
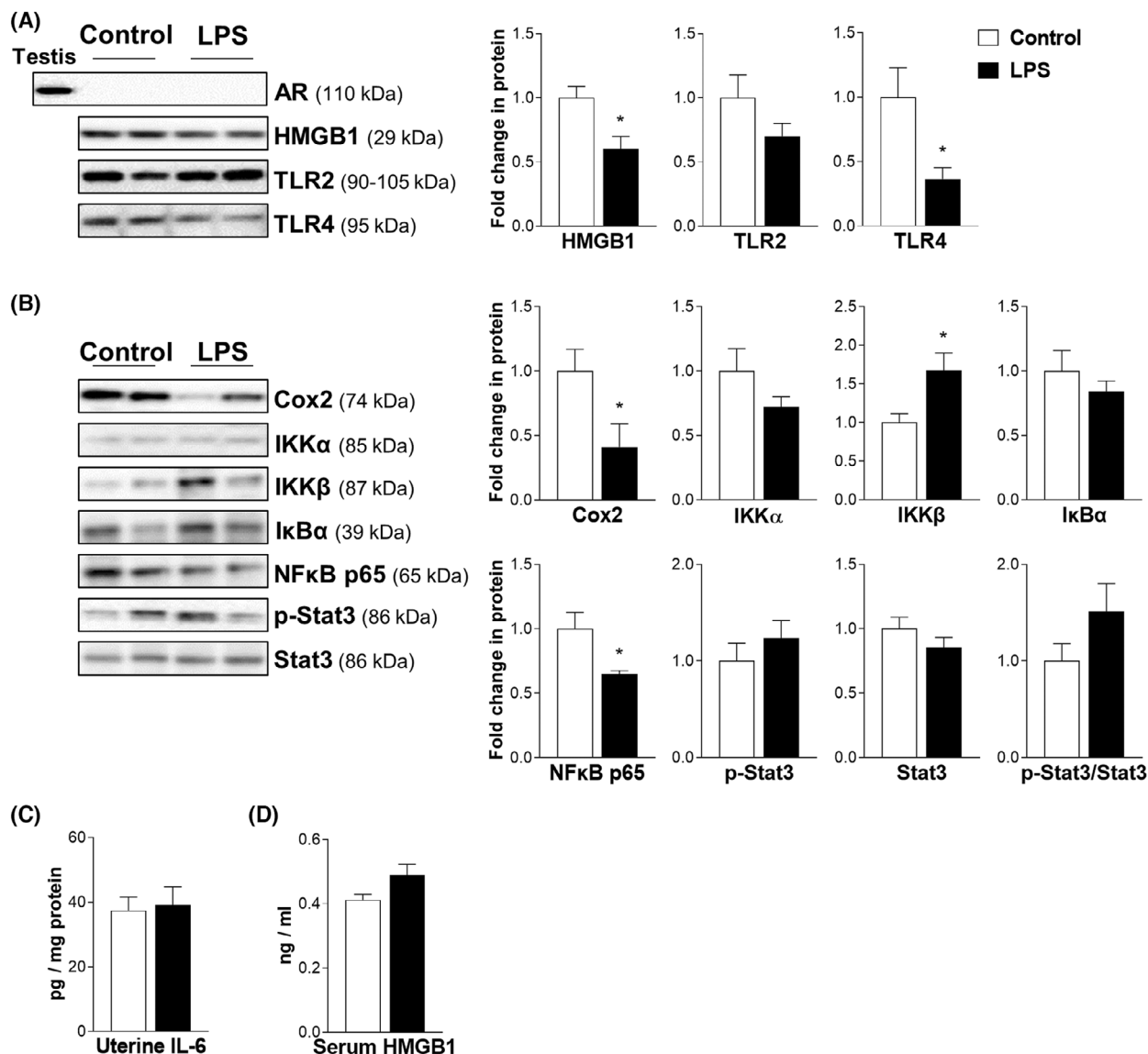
Fig. 15. The impact of LPS on uterine AR, HMGB1, TLR2 and TLR4 protein levels and NFκB signalling and pro-/anti-inflammatory protein abundance in control pregnant rats at GD 14.5. (A—C) Representative western blot from uterine lysates from control and LPS-exposed pregnant rats probed with antibodies against AR, HMGB1, TLR2 and TLR4 (A) and against Cox2, NFκB signalling molecules and Stat3 (B). (C, D) Uterine IL-6 and circulating HMGB1 levels were determined by ELISA. In all plots, data are presented as fold changes in comparison to controls (GD 14.5 values, $n = 6$ per group, each from different animals). Values are expressed as means ± SEM. Between-group comparisons were carried out by either Student's t-test or Mann–Whitney U-test, and differences between the groups are reported as *$P < 0.05$.

subcellular localization in response to insulin stimulation remains to be explored. It is worth noting that insulin resistance can aggravate hyperandrogenism in women with PCOS [1,4]. We found that non-pregnant rats exposed to hCG (referred to as elevated endogenous androgen levels [18,45]) and insulin also showed increased HMGB1 immunoreactivity in the cytoplasm of uterine epithelial cells. However, in pregnant rats, the change in HMGB1 subcellular localization in uterine epithelial cells was not significantly affected by

exposure to insulin and/or DHT. Thus, the mechanism underlying these differences remains to be elucidated. In addition, we observed that in contrast to LPS-exposed pregnant rat uteri with non-viable and resorbed fetuses, the protein abundance and/or immunoreactivities of HMGB1, TLR4, NFκB p65 and Cox2 were decreased in the LPS-exposed pregnant rat uteri with viable fetuses. Given that TLR4 is the key receptor involved in LPS recognition and signal initiation for triggering the inflammatory cascade [71], our results suggest that
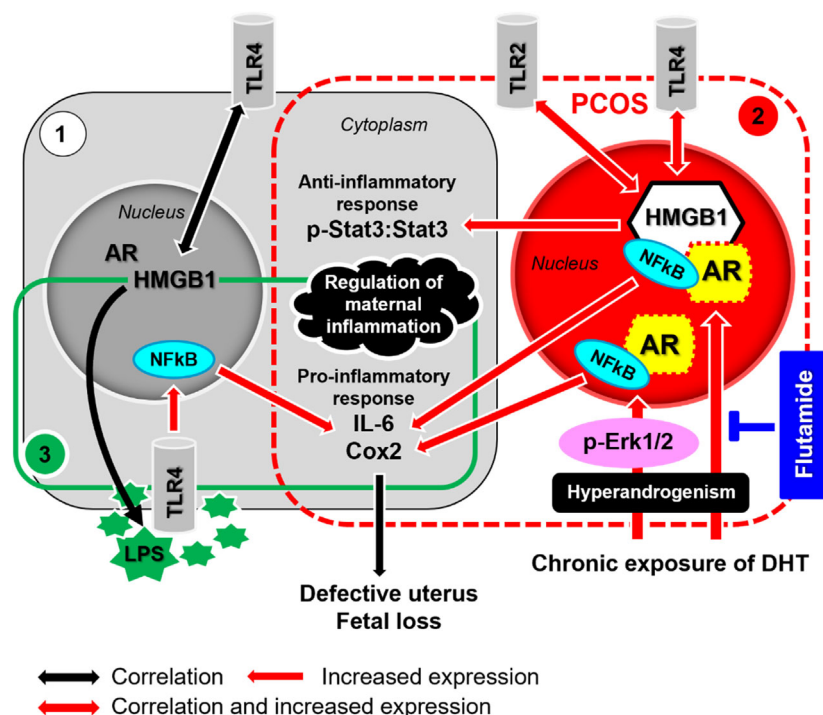
Fig. 16. Principal scheme outlining our working hypothesis regarding the mechanisms governing gravid uterine HMGB1 regulation and HMGB1-mediated inflammation and fetal loss during physiological (normal pregnancy) and pathological (PCOS and LPS) conditions. (1) There is a gestational stage-dependent decrease in HMGB1 and TLR4 abundance in the gravid uterus, which reflects the shift from the inflammatory stage to the anti-inflammatory stage during early and mid-pregnancy. (2) Combined hyperandrogenism and insulin resistance (PCOS)-induced AR activation participates in the enhancement of HMGB1/TLR2/TLR4 signalling activation and uterine inflammatory responses, while it is also likely that hyperandrogenism induces uterine inflammation through activation of Erk1/2 signalling but with no changes in HMGB1, TLR2 and TLR4 protein expression. (3) AR-independent HMGB1/TLR4 signalling activation is involved in LPS-induced uterine inflammation leading to fetal loss during pregnancy.

HMGB1-activated TLR4/NFκB/Cox2 signalling in the gravid uterus is the cause of the impaired maternal–fetal compartment, and this supports the observation that inflammation-mediated fetal loss is common in women with miscarriage (Fig. 16) [56,57,72,73].

While P4 is crucial for modulating intrauterine inflammation homeostasis during the menstrual cycle, embryo implantation and healthy pregnancy [6,8], impaired P4 response (referred to as progesterone resistance) [74] and increased expression of endometrial PR mRNAs and proteins have been found in PCOS patients [75,76]. Because P4-regulated nuclear PR exists in two isoforms (PRA and PRB) [74], changes in the relative abundance of PRA and PRB proteins may disrupt intrauterine inflammation homeostasis. For instance, in contrast to the anti-inflammatory PRB, the elevation of PRA protein expression and PRA : PRB ratio is associated with the activation of NFκB signalling and the elevation of proinflammatory gene expression in human myometrial tissue explants and myometrial cell lines [77,78]. In line with altered

gravid uterine *Pr* mRNA expression in rats [48], western blot analysis shows that exposure to DHT and insulin significantly increases uterine PRA protein expression and the PRA : PRB ratio, which can be suppressed by flutamide treatment. Although it is unknown whether the PR promotor contains specific androgen response elements, *in vitro* studies have shown that DHT up-regulates *PR* mRNA expression in an AR-dependent manner in human endometrial explants [79]. Thus, these data together with our current findings suggest that hyperandrogenism-regulated PRA may exacerbate uterine inflammation by activating the NFκB signalling pathway and subsequently result in implantation failure in PCOS-like pregnant rats. Further work might be needed to determine the precise regulatory mechanisms by which uterine PRA and AR interact and how both nuclear receptors cooperatively enhance HMGB1/TLR2/TLR4-mediated decidual inflammation during implantation and pregnancy.

One of the hallmarks of PCOS is insulin resistance, which is a manifestation of unresponsiveness,

insensitivity or both, to insulin [80]. Studies have demonstrated that the elevation of ovarian granulosa cell HMGB1 protein coincides with insulin resistance in PCOS patients [35], and suppression of HMGB1 protein ameliorates insulin resistance and restores normal insulin signalling transduction in human and mouse retinal endothelial cells [81,82]. However, the molecular defects underlying insulin resistance are metabolic tissue dependent (i.e. adipose tissues and muscle) and ovarian cell specific in PCOS patients [80]. Although we still lack a clear mechanistic understanding of how PCOS-specific insulin resistance directly causes uterine implantation failure and miscarriage, several key components of the insulin signalling transduction pathway have been demonstrated in the PCOS endometrium [75]. It is worth noting that decreased insulin sensitivity and the development of insulin resistance are seen in healthy women during the last trimester of normal pregnancy [83]. While abnormal insulin-regulated glucose-induced inflammation may directly promote hyperandrogenism, PCOS-associated hyperandrogenism can aggravate whole-body insulin resistance and *vice versa* [3,4]. These clinical observations suggest that the defective insulin signalling pathway in the reproductive tissues affected by insulin resistance and chronic insulin excess in pregnant PCOS patients is complex. Moreover, *in vitro* exposure to insulin alone or in combination with DHT suppresses human endometrial stromal cells undergoing decidualization [52]. These data corroborate our findings in pregnant rats that *in vivo* prolonged exposure to insulin and DHT impairs maternal glucose metabolism, elevated insulin resistance-related inflammatory cytokines (e.g., TNF-α and IL-6) and dysregulated expression of genes belonging to the insulin signalling pathway (Figs 6 and 11C). We, therefore, postulate that PCOS-specific insulin resistance may dysregulate the insulin signalling cascade and compromise decidual function in association with aberrant regulation of HMGB1 protein in the uterus, and this should be investigated in future studies.

Limitations of this study

The findings of this mechanistic investigation have considerably improved our understanding of how uterine HMGB1 protein expression is regulated during normal pregnancy and what the relationship is between aberrant HMGB1 protein abundance and inflammatory responses in the gravid uterus under PCOS conditions. However, our study has some limitations that can be followed up in the future. Specifically, because HMGB1 can be translocated from the nucleus into the cytoplasm, and even released into the extracellular space, in response to different pathophysiological and environmental stimuli [22,23], our current work did not demonstrate how intra-nuclear and extra-nuclear HMGB1 proteins might play different roles in inflammation-induced perturbations of uterine homeostasis during pregnancy. We used whole uterine tissues for our studies, and sample fractionation to separate the cytosolic and nuclear compartments in the uterus might be a useful additional approach in future studies. In addition, we have not tested whether suppression of HMGB1 protein expression by treatment with HMGB1 antagonists (i.e. anti-HMGB1 antibody or BoxA [23]) alters AR protein expression in the uterus. Lastly, due to the ethical impossibility of directly studying human implantation and early pregnancy, and the difficulty in obtaining the relevant uterine decidual tissues throughout normal and PCOS gestations, an important question is whether aberrant regulation of uterine HMGB1/TLR2/TLR4 proteins in our PCOS-like pregnant rat model is similarly relevant to abnormal alterations of these proteins in pregnant women with PCOS.

In summary, our study provides the first experimental insight into the pattern of uterine HMGB1, TLR2 and TLR4 protein distribution and dynamics under the conditions of hyperandrogenism and/or insulin resistance. Using an AR-specific agonist and antagonist, as well as the LPS-induced fetal loss model, we conclude that two mechanisms, namely AR-dependent and AR-independent regulation of uterine HMGB1, TLR2 and TLR4 proteins, contribute to aberrant inflammation-induced fetal loss during pregnancy. Considering that HMGB1's function is to regulate inflammatory homeostasis, embryo implantation and successful pregnancy [24,28,31], we postulate that abnormal activation of HMGB1/TLR2/TLR4 signalling results in increased uterine inflammation, which leads to defective endometrial decidua (through the disruption of endometrial receptivity and decidualization) and embryonic implantation and is thus the cause of PCOS-related adverse pregnancy outcomes, including miscarriage.

Materials and methods

Ethics approval

The research described in this study was approved by the Institutional Animal Care and Use Committee of the Heilongjiang University of Chinese Medicine, China (permit numbers: HUCM 2015-0112 and HUCM 2021-089), and followed the National Institutes of Health guidelines on the care and use of laboratory animals. All efforts were made to minimize the number and suffering of the animals used. All experiments complied with the ARRIVE guidelines 2.0 (updated guidelines for reporting animal research) [84].

For human endometrial samples [non-PCOS and PCOS patients (the proliferative phase, $n = 3$ per group)], written informed consent in compliance with the Helsinki II Declaration was obtained, and the research was approved by the institutional ethical review committee (permit number: OGHFU 2013-23) of the Obstetrics and Gynecology Hospital of Fudan University (Shanghai, China). All experimental procedures and data evaluations were performed following the relevant guidelines of this approval.

Reagents and antibodies

DHT (D-5027, an AR agonist), flutamide (F-9397, a competitive AR antagonist), lipopolysaccharide (LPS, #437629, Salmonella Minnesota Re-595) and sesame oil (S-3547) were obtained from Sigma-Aldrich (St. Louis, MO, USA). Human chorionic gonadotropin (hCG) was from NV Organon (Oss, Holland). Human recombinant insulin (INS) was obtained from Eli Lilly Pharmaceuticals (Giza, Egypt). All primary antibodies specific for different proteins were from Cell Signaling Technology (Danver, MA, USA), Abcam (Cambridge, UK) and Santa Cruz Biotechnology (Heidelberg, Germany) as indicated in Table 1. Other reagents were obtained as indicated or were of the highest purity available from commercial suppliers.

Animal care

Sprague–Dawley rats of both sexes at 70 days of age were obtained from the Laboratory Animal Centre of Harbin Medical University, Harbin, China. All animals used in this investigation were maintained under standard temperature and light cycles and with free access to a normal sterilizable diet (0% cholesterol, 0% cholic acid and 5.8% triglyceride) and water *ad libitum*. Before starting the experiments, female rats were allowed to acclimatize for a minimum of 1 week, and the stage of the oestrous cycle was monitored daily by vaginal cytology. For mating experiments, pregnancy was achieved by housing female rats on the night of proestrus with age-matched fertile males of the same strain at a 1 : 1 female-to-male ratio. The presence of a vaginal

plug and sperm in a vaginal smear the next morning was used to confirm pregnancy, and this was considered as GD 0.5. Rats were sacrificed between 8:00 AM and 10:00 AM on GD 0.5, 4.5, 7.5, 10.5 and 14.5. There was no significant difference in body weight or food intake between the different groups in the beginning of the study [48].

Experimental design

Four sets of experiments were conducted in this study.

Experiment 1

Induction of hyperandrogenism and/or insulin resistance by chronic exposure to DHT and/or insulin. Based on our previous publication [48], the pregnant rats were randomly divided into the control group (co-treatment with saline and sesame oil, $n = 24$) or the experimental group (hyperandrogenism alone, $n = 24$; insulin resistance alone, $n = 24$; hyperandrogenism and insulin resistance, $n = 24$). The control group was treated intraperitoneally (i.p.) with an equal volume of saline and sesame oil, while the experimental group was treated with DHT (1.66 mg·kg^{-1}·day^{-1} suspended in sesame oil, i.p.) alone to induce hyperandrogenism, treated with insulin (6.0 IU·day^{-1} diluted in sterile saline, i.p.) alone to induced systemic and uterine insulin resistance, or co-treated with DHT and insulin to induce hyperandrogenism and insulin resistance. All treatments were carried out from GD 0.5 to GD 13.5. The dose of DHT used in our rats was chosen to mimic the hyperandrogenic state in PCOS patients who have approximately 1.7-fold higher circulating DHT concentrations compared to healthy controls [85,86]. The dose of insulin was chosen because it induces metabolic disturbances including peripheral and uterine insulin resistance in rats [18,45,87]. The body weight was measured to confirm that combined hyperandrogenism and insulin resistance was induced by co-exposure to DHT and insulin, as reported previously [48]. For closely mimicking PCOS patient's ovarian features, pregnant rats treated chronically with DHT and insulin or DHT alone indeed exhibit decreased ovarian weight

Table 1. Sequences of primer pairs used for qPCR measurement. *Actb*, beta-actin; *Gapdh*, glyceraldehyde-3-phosphate dehydrogenase; *Ir*, insulin receptor; *Irs*, insulin receptor substrate.

Gene	Primer sequence (5′–3′)		Gene ID	Product size (bp)
Ir	Forward	CTGAAGGAGCTGGGTCTTTAC	24954	86
	Reverse	GCCAGGTAGCAGAGTTCATTAT		
Irs	Forward	GGTTTCGGAAGAGAACTCACTC	25467	112
	Reverse	GCGGGCATCATCTCTGTATATT		
Gapdh	Forward	TCTCTGCTCCTCCCTGTTCTA	24383	121
	Reverse	GGTAACCAGGCGTCCGATAC		
Actb	Forward	CGCGAGTACAACCTTCTTGC	81822	70
	Reverse	CGTCATCCATGGCGAACTGG		

and corpora lutea number along with increased cyst-like ovarian follicles [48]. In contrast to controls, long-term exposure to DHT and/or insulin dysregulated the expression of several endometrial receptivity, implantation and decidualization-related genes, whereas completely abolished embryo implantation was only observed in pregnant rats exposed to DHT and insulin or DHT alone during early and mid-pregnancy [48].

Experiment 2

Inhibition of uterine AR activation by treatment with flutamide. Flutamide (25 mg·kg^{-1}·day^{-1} suspended in 100 μL sesame oil) was injected i.p. with repeated doses from GD 0.5 to GD 13.5 in control (n = 6 per group) and DHT + INS-exposed pregnant rats (n = 6 per group). As an AR antagonist, flutamide functions by binding to the AR in competition with DHT and testosterone, and the flutamide dose was specifically chosen because it has been found to effectively improve DHT-induced defects in ovarian morphology and to restore reproductive cycles in a PCOS-like rodent model [88]. The control and DHT + INS-exposed pregnant rats (n = 6 per group) treated with 100 μL sesame oil were assigned to vehicle groups. The treatment with flutamide in DHT + INS-exposed uteri with viable fetuses was analysed. The body weight, circulating levels of androgens (testosterone, androstenedione, DHT and dehydroepiandrosterone) and oral glucose tolerance were measured to confirm that combined hyperandrogenism and insulin resistance were induced by co-exposure to DHT and insulin, as reported previously [48].

Experiment 3

Activation of uterine AR by long-term exposure to DHT. DHT was injected i.p. at 1.66 mg·kg^{-1} (n = 6), and treatment was given once a day for 13 days (from GD 0.5 to GD 13.5). The uterine tissues collected from confirmed mated rats at GD 0.5 (n = 6) were used as controls.

Experiment 4

Inflammation-induced pregnancy loss model by acute exposure to LPS. Pregnant rats (n = 10) were treated with LPS (0.25 μg·g^{-1} in 100 μL sterile normal saline as a single i.p. injection) on GD 7.5. The dose for LPS is described in detail in the original paper [72]. LPS is a component of the cell wall of Gram-negative bacteria such as *Escherichia coli*, and it stimulates inflammation and innate immunity by activation of maternal TLR4 [71]. The maternal exposure of pregnant rodents to LPS is relevant to the endometrial cytokine production and placental inflammation observed during pregnancy, which contributes to embryonic resorption and miscarriage [56,57]. Control pregnant rats (n = 10) received an equivalent volume of saline at the same GD.

Oral glucose tolerance test (OGTT)

In vivo glucose homeostasis (referred to as glucose tolerance) was assessed in pregnant rats on GD 13.5 using an OGTT as described previously [40,41]. Briefly, rats were fasted for 10 h and blood glucose concentrations were determined at 0, 30, 60, 90 and 120 min after D-glucose administration (3 g·kg^{-1} body weight in saline, oral) as a 20% wt/vol solution. Glucose concentrations were measured using a hand-held glucometer from blood sampled from the tail vein.

Tissue preparation

Animals were exposed to isoflurane (2% in a 1 : 1 mixture of oxygen to air, RWD Life Science Co., Shenzhen, China) followed by exsanguination. After carefully dissecting out the non-pregnant and pregnant uteri, placenta and fetuses, as well as the metabolic tissues (including the mesenteric adipose tissue and liver), all tissues were either fixed in 4% formaldehyde neutral-buffered solution for 24 h at 4 °C and embedded in paraffin for morphological and immunohistochemical analyses or immediately frozen in liquid nitrogen and stored at −70 °C for quantitative real-time PCR (qPCR), western blotting and co-immunoprecipitation. Only uterine tissues, mesenteric adipose tissues and livers were analysed in this study.

Additional animal and human studies

The uterine tissues in non-pregnant PCOS-like rats and in PCOS patients were collected and used as previously described in detail [18,45,46,89,90].

RNA isolation and qPCR

The isolation and quantification of the RNA and the qPCR assays were performed as previously described [41,91]. The PCR amplifications were performed with SYBR green qPCR master mix (#K0252, Thermo Scientific, Rockford, IL, USA). Total RNA was prepared from the frozen whole-uterine tissues, and single-stranded cDNA was synthesized from each sample (2 μg) with M-MLV reverse transcriptase (#0000113467, Promega Corporation, Fitchburg, WI, USA) and RNase inhibitor (40 U; #00314959, Thermo Scientific). cDNA (1 μL) was added to a reaction master mix (10 μL) containing 2× SYBR green qPCR reaction mix cocktail (Thermo Scientific) and gene-specific primers (5 μM of forward and reverse primers). The qPCR primers used in this study are listed in Table 1. All reactions were performed at least twice, and each reaction

included a non-template control. *Gapdh* and *Actb* (β-actin) were used as the internal control genes for our analysis. Fold changes in mRNA expression were calculated by the $\Delta\Delta C_T$ method, and the results are expressed as fold changes after normalizing to the average of *Gapdh* cycle threshold (C_t) and *Actb* C_t controls. All sets of primers were validated for qPCR prior to analysis. This involved determining that the efficiency of amplification using a standard curve of cDNA was above 85% and not different from the *Gapdh* and *Actb* reference genes, and there were no non-specific PCR products seen in a melting curve analysis immediately after the amplification or in parallel reactions with untranscribed RNA or in reactions without templates (the negative controls).

Protein extraction and western blot quantification

All procedures were performed as described previously [41,48]. Briefly, tissue proteins were isolated by homogenization in radioimmunoprecipitation assay lysis and extraction buffer (Sigma-Aldrich) supplemented with Roche cOmplete Mini protease inhibitor cocktail tablets (Roche Diagnostics, Mannheim, Germany) and PhosSTOP phosphatase inhibitor cocktail tablets (Roche Diagnostics). Equal amounts of protein (30 μg) were resolved on 4–20% TGX stain-free gels (Bio-Rad Laboratories GmbH,

Munich, Germany) and transferred onto Immuno-Blot polyvinylidene difluoride membranes (Bio-Rad) using the Trans-Blot® Turbo™ system (Bio-Rad) according to the manufacturer's instructions. Apparent molecular weights were determined by comparison with concurrently electrophoresed standards. Non-specific binding sites were blocked with 5% milk powder dissolved in 0.01 м Tris-buffered saline supplemented with Tween 20 (TBST) for 1 h. The membranes were probed with different primary antibodies (Table 2) in TBST containing 5% w/v non-fat dry milk followed by HRP-conjugated secondary antibody. Detection of the signal was achieved with the SuperSignal West Dura Extended Duration Substrate (Thermo Fisher Scientific, Göteborg, Sweden) according to the manufacturer's protocol and captured using a ChemiDoc MP imaging system (Bio-Rad). For each western blot, ultraviolet activation of the Criterion stain-free gel was used to assess the total protein loading for each sample. Band densitometry was performed using Image Laboratory (Version 5.0, Bio-Rad), and the intensity of each protein band was normalized to the total protein in the individual sample. For quantification and to ensure standardization across blots, the expression of the target protein was normalized to the mean value for the control group on the blot, and then all the normalized values were statistically compared to assess the effect of the treatment groups as described previously [21,48]. When necessary, the membranes were stripped

Table 2. Information of primary antibodies. AR, androgen receptor; Cox2, cyclooxygenase 2; HMGB1, high mobility group protein B1; IF, immunofluorescence; IHC, immunohistochemistry; IKKα, Ikappa B kinase, alpha; IP, immunoprecipitation; IκBα, inhibitor of nuclear factor kappa B, alpha; NFκB p65, nuclear factor-kB activation p65; p-Erk1/2, phosphorylated extracellular signal-regulated kinases 1/2; PR, progesterone receptor; p-Stat3, phosphorylated signal transducer and activator of transcription 3; TLR2, toll-like receptor 2; WB, western blot analysis.

Antibody	Species	Catalogue number/clone	Method	Dilution	Company
HMGB1	Rabbit	6893/D3E5	WB	1 : 1000	Cell Signaling Technology (Danver, MA, USA)
			IHC	1 : 200	
TLR2	Rabbit	213 676	WB	1 : 1000	Abcam (Cambridge, UK)
TLR4	Rabbit	13 556	WB	1 : 1000	Abcam
AR	Rabbit	133 273/EPR1535(2)	WB	1 : 1000	Abcam
			IF	1 : 200	
AR	Mouse	sc-7305/441	IP	1 : 50	Santa Cruz Biotechnology (Heidelberg, Germany)
			WB	1 : 200	
Cox2	Rabbit	12 282/D5H5	WB	1 : 500	Cell Signaling Technology
PR	Mouse	MA1-410	WB	1 : 500	Thermo Fisher (Rockford, IL, USA)
IKKα	Mouse	11 930/3G12	WB	1 : 1000	Cell Signaling Technology
IKKβ	Rabbit	8943/D30C6	WB	1 : 1000	Cell Signaling Technology
IκBα	Mouse	4814/L35A5	WB	1 : 1000	Cell Signaling Technology
NFκB p65	Rabbit	8242/D14E12	WB	1 : 1000	Cell Signaling Technology
			IHC	1 : 200	
p-Stat3	Rabbit	9145/D3A7	WB	1 : 500	Cell Signaling Technology
Stat3	Rabbit	8768/D1A5	WB	1 : 1000	Cell Signaling Technology
p-Erk1/2	Rabbit	4370/D13.14.4 E	WB	1 : 500	Cell Signaling Technology
Erk1/2	Rabbit	4695/137F5	WB	1 : 2000	Cell Signaling Technology
Cleaved-caspase-3	Rabbit	9664/5A1E	IF	1 : 200	Cell Signaling Technology

using Restore PLUS western blot stripping buffer (Thermo Fisher Scientific) for 15 min at room temperature, washed three times in TBST and then re-probed [40,41,48].

Pulldown from tissue lysates and immunoprecipitation

All procedures were performed as described previously [21]. Briefly, uterine tissues were extracted with ice-cold lysis buffer. Either anti-AR or anti-HMGB1 antibody (Table 2) or the rabbit IgG isotype (02-6102, Thermo Fisher Scientific) was added to 50 μg protein extracts and incubated at 4 °C overnight on a rotating wheel. The resulting immobilized immune complexes were collected on protein G plus/protein A agarose beads (IP05, EMD Millipore Corp., Burlington, CA, USA) by centrifugation at 4 °C and then washed with lysis buffer supplemented with Roche cOmplete Mini protease inhibitor cocktail tablets. The bound protein was eluted by boiling in SDS sample-reducing loading buffer (Bio-Rad) for 5 min and then loaded onto the same gels that were run at the same time within the same electrophoresis unit and examined by western blotting as described above.

Immunohistochemistry and immunofluorescence microscopy

After fixing in 4% formaldehyde neutral-buffered solution and embedding in paraffin, the rat uterine and human endometrial tissues were sectioned for haematoxylin and eosin (H&E) staining according to standard procedures. Immunohistochemistry was conducted according to previously published methods [41,48]. Briefly, formalin-fixed sections (5 μm) were deparaffinized in graded xylene and alcohol and rinsed in 10 mM sodium citrate buffer (pH 6.0). For antigen retrieval, slides were heated in a microwave oven (10 min at 700 W) and cooled to room temperature in a buffer bath. The endogenous peroxidase activity was blocked by incubating with 3% hydrogen peroxide in phosphate-buffered saline for 20 min. After incubation with anti-HMGB1 antibody or anti-NFκB antibody (Table 2) overnight at 4 °C in a humidified chamber, the sections were stained using the avidin-biotinylated peroxidase ABC kit followed by a 5-min treatment with 3,3′-diaminobenzidine (SK-4100, Vector Laboratories, Burlingame, CA, USA) as the chromogen. All sections were further counterstained with eosin or methyl green (H-3402, Vector Laboratories) according to the manufacturer's instructions. After washing, all slides were dehydrated and mounted in xylene mountant. Stained sections were observed and imaged on a Nikon E-1000 microscope (Japan) under bright-field optics and photomicrographed using Easy Image 1 (Bergström Instrument AB, Stockholm, Sweden). The optimal concentration of anti-HMGB1 antibody was determined in initial experiments. The negative controls received the same concentration of normal rabbit IgG instead of the primary antibody. Additional control sections were processed as above, but with the omission of either the primary or secondary antibody (Figs 2 and 3). Little or no background cytoplasmic immunostaining was observed.

Immunofluorescence staining was conducted according to a previously published method [46,91]. The uterine tissue sections were incubated with anti-cleaved caspase-3 antibody or anti-AR antibody (Table 1) in TBST (TBS supplemented with Triton-100) containing 5% non-fat milk overnight at 4 °C in a humidified chamber, followed by an Alexa Fluor-conjugated secondary antibody for 1 h at room temperature. After the sections were washed with TBST, they were mounted in a mounting medium containing DAPI (4′,6′-diamidino-2-phenylindole; Vector Laboratories), coverslipped and examined under an Axiovert 200 confocal fluorescence microscope (Zeiss, Jena, Germany) equipped with a laser-scanning confocal imaging LSM 710 META system (Carl Zeiss). The same concentration of normal rabbit IgG instead of the primary and secondary antibodies was used as the negative control. Background settings were adjusted from the examination of negative control specimens. Images of positive staining were adjusted to make optimal use of the dynamic range of detection.

Determination of tissue interleukin 6 (IL-6) content

The intracellular IL-6 level was determined by enzyme-linked immunosorbent assay (ELISA) using the rat IL-6 assay kit (RAB0312, Millipore-Sigma-Aldrich) according to the manufacturer's instructions. The intra- and inter-assay coefficients of variation of the IL-6 assay were 10% and 12% respectively. A standard curve for IL-6 concentration was generated and used for calculating IL-6 concentrations in the samples. The concentration of IL-6 in each group was normalized to the total uterine tissue protein concentration as determined by the Bradford protein assay (Thermo Fisher Scientific).

Determination of circulating HMGB1 and tumour necrosis factor alpha (TNF-α) levels

The circulating levels of HMGB1 and TNF-α were determined using the rat HMGB1 ELISA kit (ARG81310, Arigo, Taiwan, China) and rat TNF-α ELISA kit (YJ002859, Mlbio, Shanghai, China) according to the manufacturers' instructions. The intra- and inter-assay coefficients of variation of the HMGB1 and TNF-α assays were 4.3%/5.2% and < 10%/15% respectively. A standard curve for HMGB1 and TNF-α concentration was generated and used for calculating their concentrations in the samples.

Measurement of biochemical parameters

The concentrations of serum hormones [total testosterone (T), androstenedione (A4), DHT, dehydroepiandrosterone

(DHEA), sex hormone-binding globulin (SHBG), anti-Mullerian hormone (AMH), progesterone (P4) and 17β-oestradiol (E2)] were quantified by chemiluminescence (Beckman Coulter, Inc., California, CA, USA and Abbott Laboratories, Chicago, IL, USA). The reproducibility (intra-/inter-assay coefficients of variation) of rat T, A4, DHT, DHEA, SHBG, AMH, P4 and E2 were 6.2%/6.6%, 6.7%/6.9%, 6.2%/6.7%, 6.3%/6.6%, 6.4%/6.8%, 6.5%/6.7%, 6.4%/6.6% and 6.5%/6.8% respectively.

Data analysis and statistics

All analyses and graphs were performed using SPSS version 24.0 (SPSS Inc., Chicago, IL, USA) and GRAPHPAD PRISM 9.0 (GraphPad Software, San Diego, CA, USA). The normal distribution of the data was tested with the Shapiro–Wilk test. For the time-course studies, data were analysed with two-way ANOVA (including the factors of GD and hormonal treatment) followed by pair-wise Tukey's *post hoc* tests. The main effects of GD and/or hormonal treatment are referred to as P_{GD}, P_{treat} and $P_{GD:treat}$ respectively. For the systemic treatment experiments using the AR antagonist flutamide, DHT and LPS, normally distributed data were analysed by one-way ANOVA followed by Tukey's *post hoc* test or Student's *t*-test. Data that were not normally distributed were tested for statistical significance between groups with the Kruskal–Wallis test or Mann–Whitney *U*-test. Pearson's correlation coefficient was used to examine the strength of the associations between HMGB1 and TLR2/4 protein expression in the gravid uterus from control pregnant rats exposed to DHT and/or INS from GD 4.5 to GD 14.5. All values are reported as means ± standard error. The sample size (*n*) was chosen based on standard experimental requirements in molecular biology and is indicated in the figure legends. Significance for all comparisons was accepted at $P < 0.05$.

Acknowledgements

Conflict of interest

The authors declare no conflict of interest.

Author contributions

LRS conceptualized, designed and supervised the project; MH, YZ, YL, JH, TG, PC and LRS carried out the research and analysed the data; MH, YZ and LRS elaborated the manuscript and prepared the figures; and MB, LRS and HB contributed to discussion and reviewed and edited the manuscript. MH, YZ, LRS and HB are the guarantors of this work and, as such, had full access to all the data in the study and take responsibility for the integrity of the data and the accuracy of the data analysis. All authors have read and approved the final version of the manuscript.

Data availability statement

All data needed to evaluate the conclusions in this study are present in the article. The data that support the findings of this study are available from the corresponding author upon reasonable request.

References

1 Hoeger KM, Dokras A, Piltonen T. Update on PCOS: consequences, challenges, and guiding treatment. *J Clin Endocrinol Metab*. 2021;**106**:e1071–83.

2 Wolf WM, Wattick RA, Kinkade ON, Olfert MD. Geographical prevalence of polycystic ovary syndrome as determined by region and race/ethnicity. *Int J Environ Res Public Health*. 2018;**15**:2589.

3 Azziz R, Carmina E, Chen Z, Dunaif A, Laven JS, Legro RS, et al. Polycystic ovary syndrome. *Nat Rev Dis Primers*. 2016;**2**:16057.

4 Escobar-Morreale HF. Polycystic ovary syndrome: definition, aetiology, diagnosis and treatment. *Nat Rev Endocrinol.* 2018;**14**:270–84.

5 Palomba S, de Wilde MA, Falbo A, Koster MP, La Sala GB, Fauser BC. Pregnancy complications in women with polycystic ovary syndrome. *Hum Reprod Update.* 2015;**21**:575–92.

6 Palomba S, Piltonen TT, Giudice LC. Endometrial function in women with polycystic ovary syndrome: a comprehensive review. *Hum Reprod Update.* 2021;**27**:584–618.

7 Palomba S. Is fertility reduced in ovulatory women with polycystic ovary syndrome? An opinion paper. *Hum Reprod.* 2021;**36**:2421–8.

8 Osokine I, Erlebacher A. Immunology of the decidua. In: Mor G, editor. Reproductive immunology: basic concepts. Andre Gerhard Wolff, Academic Press (Elsevier), India; 2021. p. 129–46.

9 Schatz F, Guzeloglu-Kayisli O, Arlier S, Kayisli UA, Lockwood CJ. The role of decidual cells in uterine hemostasis, menstruation, inflammation, adverse pregnancy outcomes and abnormal uterine bleeding. *Hum Reprod Update.* 2016;**22**:497–515.

10 Negishi Y, Shima Y, Takeshita T, Morita R. Harmful and beneficial effects of inflammatory response on reproduction: sterile and pathogen-associated inflammation. *Immunol Med.* 2021;**44**:98–115.

11 Velez LM, Seldin M, Motta AB. Inflammation and reproductive function in women with polycystic ovary syndromedagger. *Biol Reprod.* 2021;**104**:1205–17.

12 Beharier O, Kajiwara K, Sadovsky Y. Ferroptosis, trophoblast lipotoxic damage, and adverse pregnancy outcome. *Placenta.* 2021;**108**:32–8.

13 Patel S. Polycystic ovary syndrome (PCOS), an inflammatory, systemic, lifestyle endocrinopathy. *J Steroid Biochem Mol Biol.* 2018;**182**:27–36.

14 Gonzalez F, Sia CL, Bearson DM, Blair HE. Hyperandrogenism induces a proinflammatory TNFalpha response to glucose ingestion in a receptor-dependent fashion. *J Clin Endocrinol Metab.* 2014;**99**: E848–54.

15 Hu M, Zhang Y, Li X, Cui P, Sferruzzi-Perri AN, Brannstrom M, et al. TLR4-associated IRF-7 and NFkappaB signaling act as a molecular link between androgen and metformin activities and cytokine synthesis in the PCOS endometrium. *J Clin Endocrinol Metab.* 2021;**106**:1022–40.

16 Li Y, Zheng Q, Sun D, Cui X, Chen S, Bulbul A, et al. Dehydroepiandrosterone stimulates inflammation and impairs ovarian functions of polycystic ovary syndrome. *J Cell Physiol.* 2019;**234**:7435–47.

17 Gonzalez F, Considine RV, Abdelhadi OA, Acton AJ. Saturated fat ingestion promotes lipopolysaccharide-mediated inflammation and insulin resistance in polycystic ovary syndrome. *J Clin Endocrinol Metab.* 2019;**104**:934–46.

18 Zhang Y, Hu M, Meng F, Sun X, Xu H, Zhang J, et al. Metformin ameliorates uterine defects in a rat model of polycystic ovary syndrome. *EBioMedicine.* 2017;**18**:157–70.

19 Zhang Y, Hu M, Jia W, Liu G, Zhang J, Wang B, et al. Hyperandrogenism and insulin resistance modulate gravid uterine and placental ferroptosis in PCOS-like rats. *J Endocrinol.* 2020;**246**:247–63.

20 Hu M, Zhang Y, Ma S, Li J, Wang X, Liang M, et al. Suppression of uterine and placental ferroptosis by N-acetylcysteine in a rat model of polycystic ovary syndrome. *Mol Hum Reprod.* 2021;**27**:gaab067.

21 Hu M, Zhang Y, Lu L, Zhou Y, Wu D, Brannstrom M, et al. Overactivation of the androgen receptor exacerbates gravid uterine ferroptosis via interaction with and suppression of the NRF2 defense signaling pathway. *FEBS Lett.* 2022;**596**:806–25.

22 Chen R, Kang R, Tang D. The mechanism of HMGB1 secretion and release. *Exp Mol Med.* 2022;**54**:91–102.

23 Kang R, Chen R, Zhang Q, Hou W, Wu S, Cao L, et al. HMGB1 in health and disease. *Mol Aspects Med.* 2014;**40**:1–116.

24 Saito Reis CA, Padron JG, Norman Ing ND, Kendal-Wright CE. High-mobility group box 1 is a driver of inflammation throughout pregnancy. *Am J Reprod Immunol.* 2021;**85**:e13328.

25 Yang H, Wang H, Chavan SS, Andersson U. High mobility group box protein 1 (HMGB1): the prototypical endogenous danger molecule. *Mol Med.* 2015;**21**(Suppl 1):S6–12.

26 Khambu B, Huda N, Chen X, Antoine DJ, Li Y, Dai G, et al. HMGB1 promotes ductular reaction and tumorigenesis in autophagy-deficient livers. *J Clin Invest.* 2018;**128**:2419–35.

27 Hreggvidsdottir HS, Ostberg T, Wahamaa H, Schierbeck H, Aveberger AC, Klevenvall L, et al. The alarmin HMGB1 acts in synergy with endogenous and exogenous danger signals to promote inflammation. *J Leukoc Biol.* 2009;**86**:655–62.

28 Bhutada S, Basak T, Savardekar L, Katkam RR, Jadhav G, Metkari SM, et al. High mobility group box 1 (HMGB1) protein in human uterine fluid and its relevance in implantation. *Hum Reprod.* 2014;**29**:763–80.

29 Yun BH, Chon SJ, Choi YS, Cho S, Lee BS, Seo SK. Pathophysiology of endometriosis: role of high mobility group Box-1 and toll-like receptor 4 developing inflammation in endometrium. *PLoS ONE.* 2016;**11**: e0148165.

30 Wang K, Yang ZQ, Yu HF, Wang YS, Guo B, Yue ZP. High mobility group box 1 regulates uterine decidualization through bone morphogenetic protein 2 and plays a role in Kruppel-like factor 5-induced

stromal differentiation. *Cell Physiol Biochem.* 2018;**48**:2399–408.

31 Aikawa S, Deng W, Liang X, Yuan J, Bartos A, Sun X, et al. Uterine deficiency of high-mobility group box-1 (HMGB1) protein causes implantation defects and adverse pregnancy outcomes. *Cell Death Differ.* 2020;**27**:1489–504.

32 Zhu D, Zou H, Liu J, Wang J, Ma C, Yin J, et al. Inhibition of HMGB1 ameliorates the maternal-fetal Interface destruction in unexplained recurrent spontaneous abortion by suppressing Pyroptosis activation. *Front Immunol.* 2021;**12**:782792.

33 Jiang B, Xue M, Xu D, Song Y, Zhu S. Upregulation of microRNA-204 improves insulin resistance of polycystic ovarian syndrome via inhibition of HMGB1 and the inactivation of the TLR4/NF-kappaB pathway. *Cell Cycle.* 2020;**19**:697–710.

34 Zhu HL, Chen YQ, Zhang ZF. Downregulation of lncRNA ZFAS1 and upregulation of microRNA-129 repress endocrine disturbance, increase proliferation and inhibit apoptosis of ovarian granulosa cells in polycystic ovarian syndrome by downregulating HMGB1. *Genomics.* 2020;**112**:3597–608.

35 Zhang C, Hu J, Wang W, Sun Y, Sun K. HMGB1-induced aberrant autophagy contributes to insulin resistance in granulosa cells in PCOS. *FASEB J.* 2020;**34**:9563–74.

36 Cirillo F, Catellani C, Sartori C, Lazzeroni P, Morini D, Nicoli A, et al. CFTR and FOXO1 gene expression are reduced and high mobility group box 1 (HMGB1) is increased in the ovaries and serum of women with polycystic ovarian syndrome. *Gynecol Endocrinol.* 2019;**35**:842–6.

37 Wang HH, Lin M, Xiang GD. Serum HMGB1 levels and its association with endothelial dysfunction in patients with polycystic ovary syndrome. *Physiol Res.* 2018;**67**:911–9.

38 Cirillo F, Catellani C, Lazzeroni P, Sartori C, Tridenti G, Vezzani C, et al. HMGB1 is increased in adolescents with polycystic ovary syndrome (PCOS) and decreases after treatment with MYO-inositol (MYO) in combination with alpha-lipoic acid (ALA). *Gynecol Endocrinol.* 2020;**36**:588–93.

39 Ni XR, Sun ZJ, Hu GH, Wang RH. High concentration of insulin promotes apoptosis of primary cultured rat ovarian granulosa cells via its increase in extracellular HMGB1. *Reprod Sci.* 2015;**22**:271–7.

40 Zhang Y, Zhao W, Xu H, Hu M, Guo X, Jia W, et al. Hyperandrogenism and insulin resistance-induced fetal loss: evidence for placental mitochondrial abnormalities and elevated reactive oxygen species production in pregnant rats that mimic the clinical features of polycystic ovary syndrome. *J Physiol.* 2019;**597**:3927–50.

41 Hu M, Zhang Y, Guo X, Jia W, Liu G, Zhang J, et al. Hyperandrogenism and insulin resistance induce gravid

uterine defects in association with mitochondrial dysfunction and aberrant ROS production. *Am J Physiol Endocrinol Metab.* 2019;**316**:E794–809.

42 Gong H, Wu W, Xu J, Yu D, Qiao B, Liu H, et al. Flutamide ameliorates uterine decidualization and angiogenesis in the mouse hyperandrogenemia model during mid-pregnancy. *PLoS ONE.* 2019;**14**:e0217095.

43 Ojeda-Ojeda M, Martinez-Garcia MA, Alpanes M, Luque-Ramirez M, Escobar-Morreale HF. Association of TLR2 S450S and ICAM1 K469E polymorphisms with polycystic ovary syndrome (PCOS) and obesity. *J Reprod Immunol.* 2016;**113**:9–15.

44 Koga K, Izumi G, Mor G, Fujii T, Osuga Y. Toll-like receptors at the maternal-fetal interface in normal pregnancy and pregnancy complications. *Am J Reprod Immunol.* 2014;**72**:192–205.

45 Zhang Y, Sun X, Sun X, Meng F, Hu M, Li X, et al. Molecular characterization of insulin resistance and glycolytic metabolism in the rat uterus. *Sci Rep.* 2016;**6**:30679.

46 Hu M, Zhang Y, Li X, Cui P, Li J, Brannstrom M, et al. Alterations of endometrial epithelial-mesenchymal transition and MAPK signalling components in women with PCOS are partially modulated by metformin in vitro. *Mol Hum Reprod.* 2020;**26**:312–26.

47 Hu M, Zhang Y, Guo X, Jia W, Liu G, Zhang J, et al. Perturbed ovarian and uterine glucocorticoid receptor signaling accompanies the balanced regulation of mitochondrial function and NFkappaB-mediated inflammation under conditions of hyperandrogenism and insulin resistance. *Life Sci.* 2019;**232**:116681.

48 Zhang Y, Hu M, Yang F, Zhang Y, Ma S, Zhang D, et al. Increased uterine androgen receptor protein abundance results in implantation and mitochondrial defects in pregnant rats with hyperandrogenism and insulin resistance. *J Mol Med (Berl).* 2021;**99**:1427–46.

49 Maliqueo M, Lara HE, Sanchez F, Echiburu B, Crisosto N, Sir-Petermann T. Placental steroidogenesis in pregnant women with polycystic ovary syndrome. *Eur J Obstet Gynecol Reprod Biol.* 2013;**166**:151–5.

50 Sir-Petermann T, Maliqueo M, Angel B, Lara HE, Perez-Bravo F, Recabarren SE. Maternal serum androgens in pregnant women with polycystic ovarian syndrome: possible implications in prenatal androgenization. *Hum Reprod.* 2002;**17**:2573–9.

51 Cornillie FJ, Lauweryns JM, Brosens IA. Normal human endometrium. An ultrastructural survey. *Gynecol Obstet Invest.* 1985;**20**:113–29.

52 Hirschberg AL, Jakson I, Graells Brugalla C, Salamon D, Ujvari D. Interaction between insulin and androgen signalling in decidualization, cell migration and trophoblast invasion in vitro. *J Cell Mol Med.* 2021;**25**:9523–32.

53 Younas K, Quintela M, Thomas S, Garcia-Parra J, Blake L, Whiteland H, et al. Delayed endometrial

decidualisation in polycystic ovary syndrome; the role of AR-MAGEA11. *J Mol Med (Berl)*. 2019;**97**:1315–27.

54 Rostamtabar M, Esmaeilzadeh S, Tourani M, Rahmani A, Baee M, Shirafkan F, et al. Pathophysiological roles of chronic low-grade inflammation mediators in polycystic ovary syndrome. *J Cell Physiol*. 2021;**236**:824–38.

55 Thiebaut C, Vlaeminck-Guillem V, Tredan O, Poulard C, Le Romancer M. Non-genomic signaling of steroid receptors in cancer. *Mol Cell Endocrinol*. 2021;**538**:111453.

56 Moustafa S, Joseph DN, Taylor RN, Whirledge S. New models of lipopolysaccharide-induced implantation loss reveal insights into the inflammatory response. *Am J Reprod Immunol*. 2019;**81**:e13082.

57 Renaud SJ, Cotechini T, Quirt JS, Macdonald-Goodfellow SK, Othman M, Graham CH. Spontaneous pregnancy loss mediated by abnormal maternal inflammation in rats is linked to deficient uteroplacental perfusion. *J Immunol*. 2011;**186**:1799–808.

58 Falcón BJ, Cotechini T, Macdonald-Goodfellow SK, Othman M, Graham CH. Abnormal inflammation leads to maternal coagulopathies associated with placental haemostatic alterations in a rat model of foetal loss. *Thromb Haemost*. 2012;**107**:438–47.

59 Khatun M, Meltsov A, Lavogina D, Loid M, Kask K, Arffman RK, et al. Decidualized endometrial stromal cells present with altered androgen response in PCOS. *Sci Rep*. 2021;**11**:16287.

60 Diao HL, Su RW, Tan HN, Li SJ, Lei W, Deng WB, et al. Effects of androgen on embryo implantation in the mouse delayed-implantation model. *Fertil Steril*. 2008;**90**:1376–83.

61 Gibson DA, Simitsidellis I, Saunders PT. Regulation of androgen action during establishment of pregnancy. *J Mol Endocrinol*. 2016;**57**:R35–47.

62 Elenis E, Desroziers E, Persson S, Sundstrom Poromaa I, Campbell RE. Early initiation of anti-androgen treatment is associated with increased probability of spontaneous conception leading to childbirth in women with polycystic ovary syndrome: a population-based multiregistry cohort study in Sweden. *Hum Reprod*. 2021;**36**:1427–35.

63 Boonyaratanakornkit V, Melvin V, Prendergast P, Altmann M, Ronfani L, Bianchi ME, et al. High-mobility group chromatin proteins 1 and 2 functionally interact with steroid hormone receptors to enhance their DNA binding in vitro and transcriptional activity in mammalian cells. *Mol Cell Biol*. 1998;**18**:4471–87.

64 Verrijdt G, Haelens A, Schoenmakers E, Rombauts W, Claessens F. Comparative analysis of the influence of the high-mobility group box 1 protein on DNA binding and transcriptional activation by the androgen, glucocorticoid, progesterone and mineralocorticoid receptors. *Biochem J*. 2002;**361**:97–103.

65 Ujvari D, Hulchiy M, Calaby A, Nybacka A, Bystrom B, Hirschberg AL. Lifestyle intervention up-regulates gene and protein levels of molecules involved in insulin signaling in the endometrium of overweight/obese women with polycystic ovary syndrome. *Hum Reprod*. 2014;**29**:1526–35.

66 Fornes R, Ormazabal P, Rosas C, Gabler F, Vantman D, Romero C, et al. Changes in the expression of insulin signaling pathway molecules in endometria from polycystic ovary syndrome women with or without hyperinsulinemia. *Mol Med*. 2010;**16**:129–36.

67 Qi J, Wang W, Zhu Q, He Y, Lu Y, Wang Y, et al. Local cortisol elevation contributes to endometrial insulin resistance in polycystic ovary syndrome. *J Clin Endocrinol Metab*. 2018;**103**:2457–67.

68 Orostica L, Astorga I, Plaza-Parrochia F, Vera C, Garcia V, Carvajal R, et al. Proinflammatory environment and role of TNF-alpha in endometrial function of obese women having polycystic ovarian syndrome. *Int J Obes (Lond)*. 2016;**40**:1715–22.

69 Piltonen TT, Chen JC, Khatun M, Kangasniemi M, Liakka A, Spitzer T, et al. Endometrial stromal fibroblasts from women with polycystic ovary syndrome have impaired progesterone-mediated decidualization, aberrant cytokine profiles and promote enhanced immune cell migration in vitro. *Hum Reprod*. 2015;**30**:1203–15.

70 Piltonen TT, Chen J, Erikson DW, Spitzer TL, Barragan F, Rabban JT, et al. Mesenchymal stem/progenitors and other endometrial cell types from women with polycystic ovary syndrome (PCOS) display inflammatory and oncogenic potential. *J Clin Endocrinol Metab*. 2013;**98**:3765–75.

71 Brown AG, Maubert ME, Anton L, Heiser LM, Elovitz MA. The tracking of lipopolysaccharide through the feto-maternal compartment and the involvement of maternal TLR4 in inflammation-induced fetal brain injury. *Am J Reprod Immunol*. 2019;**82**:e13189.

72 Deb K, Chaturvedi MM, Jaiswal YK. A 'minimum dose' of lipopolysaccharide required for implantation failure: assessment of its effect on the maternal reproductive organs and interleukin-1alpha expression in the mouse. *Reproduction*. 2004;**128**:87–97.

73 Silver RM, Edwin SS, Trautman MS, Simmons DL, Branch DW, Dudley DJ, et al. Bacterial lipopolysaccharide-mediated fetal death. Production of a newly recognized form of inducible cyclooxygenase (COX-2) in murine decidua in response to lipopolysaccharide. *J Clin Invest*. 1995;**95**:725–31.

74 Li X, Feng Y, Lin JF, Billig H, Shao R. Endometrial progesterone resistance and PCOS. *J Biomed Sci*. 2014;**21**:2.

75 Piltonen TT. Polycystic ovary syndrome: endometrial markers. *Best Pract Res Clin Obstet Gynaecol*. 2016;**37**:66–79.

76 Hu M, Li J, Zhang Y, Li X, Brannstrom M, Shao LR, et al. Endometrial progesterone receptor isoforms in women with polycystic ovary syndrome. *Am J Transl Res*. 2018;**10**:2696–705.

77 Tan H, Yi L, Rote NS, Hurd WW, Mesiano S. Progesterone receptor-a and -B have opposite effects on proinflammatory gene expression in human myometrial cells: implications for progesterone actions in human pregnancy and parturition. *J Clin Endocrinol Metab*. 2012;**97**:E719–30.

78 Peters GA, Yi L, Skomorovska-Prokvolit Y, Patel B, Amini P, Tan H, et al. Inflammatory stimuli increase progesterone receptor-a stability and Transrepressive activity in myometrial cells. *Endocrinology*. 2017;**158**:158–69.

79 Babayev SN, Park CW, Keller PW, Carr BR, Word RA, Bukulmez O. Androgens upregulate endometrial epithelial progesterone receptor expression: potential implications for endometriosis. *Reprod Sci*. 2017;**24**:1454–61.

80 Diamanti-Kandarakis E, Papavassiliou AG. Molecular mechanisms of insulin resistance in polycystic ovary syndrome. *Trends Mol Med*. 2006;**12**:324–32.

81 Liu L, Jiang Y, Steinle JJ. Inhibition of HMGB1 protects the retina from ischemia-reperfusion, as well as reduces insulin resistance proteins. *PLoS ONE*. 2017;**12**: e0178236.

82 Jiang Y, Steinle JJ. HMGB1 inhibits insulin signalling through TLR4 and RAGE in human retinal endothelial cells. *Growth Factors*. 2018;**36**:164–71.

83 Butte NF. Carbohydrate and lipid metabolism in pregnancy: normal compared with gestational diabetes mellitus. *Am J Clin Nutr*. 2000;**71**:1256S–61S.

84 Percie du Sert N, Hurst V, Ahluwalia A, Alam S, Avey MT, Baker M, et al. The ARRIVE guidelines 2.0: updated guidelines for reporting animal research. *J Physiol*. 2020;**598**:3793–801.

85 Silfen ME, Denburg MR, Manibo AM, Lobo RA, Jaffe R, Ferin M, et al. Early endocrine, metabolic, and sonographic characteristics of polycystic ovary syndrome (PCOS): comparison between nonobese and obese adolescents. *J Clin Endocrinol Metab*. 2003;**88**:4682–8.

86 Fassnacht M, Schlenz N, Schneider SB, Wudy SA, Allolio B, Arlt W. Beyond adrenal and ovarian androgen generation: increased peripheral 5 alpha-reductase activity in women with polycystic ovary syndrome. *J Clin Endocrinol Metab*. 2003;**88**:2760–6.

87 Zhang Y, Meng F, Sun X, Sun X, Hu M, Cui P, et al. Hyperandrogenism and insulin resistance contribute to hepatic steatosis and inflammation in female rat liver. *Oncotarget*. 2018;**9**:18180–97.

88 Silva MS, Prescott M, Campbell RE. Ontogeny and reversal of brain circuit abnormalities in a preclinical model of PCOS. *JCI Insight*. 2018;**3**:e99405.

89 Li X, Pishdari B, Cui P, Hu M, Yang HP, Guo YR, et al. Regulation of androgen receptor expression alters AMPK phosphorylation in the endometrium: in vivo and in vitro studies in women with polycystic ovary syndrome. *Int J Biol Sci*. 2015;**11**:1376–89.

90 Cui P, Hu W, Ma T, Hu M, Tong X, Zhang F, et al. Long-term androgen excess induces insulin resistance and non-alcoholic fatty liver disease in PCOS-like rats. *J Steroid Biochem Mol Biol*. 2021;**208**:105829.

91 Hu M, Zhang Y, Feng J, Xu X, Zhang J, Zhao W, et al. Uterine progesterone signaling is a target for metformin therapy in PCOS-like rats. *J Endocrinol*. 2018;**237**:123–37.